SPACE - CHARGE - LIMITED CURRENT

in

FAST NEUTRON IRRADIATED SILICON

Thesis by

Quat Thuong Vu

In Partial Fulfillment of the Requirements

For the Degree of

Doctor of Philosophy

California Institute of Technology

Pasadena, California

1970

(Submitted April 2, 1970)

ACKNOWLEDGMENTS

I am deeply indebted to Dr. Marc-A. Nicolet for his great patience, understanding and careful guidance during the course of this work. Special thanks go to Dr. J. W. Mayer for his many suggestions and comments in the writing of the manuscript.

I am very grateful to D. Gollnick of the California State College at Los Angeles who performed the irradiations and to Dr. J. L. Shapiro of the California Institute of Technology who conducted the activation analyses of the foils. The financial support of the Agency for International Development is greatly appreciated. This work was also supported by the NASA Electronics Research Center, Cambridge, Massachusetts.

I would like to thank Miss Carolyn Elsbree for typing the manuscript and Mrs. Paula Clark-Samazan for help in the library and for many conversations full of funny anecdotes throughout the years spent on this work.

Kính tặng thầy

To C. M. S.

ABSTRACT

DC and transient measurements of space-charge-limited currents through alloyed and symmetrical $n^+ \nu\ n^+$ structures made of nominally 75 kΩcm ν-type silicon are studied before and after the introduction of defects by 14 MeV neutron radiation. In the transient measurements, the current response to a large turn-on voltage step is analyzed. Right after the voltage step is applied, the current transient reaches a value which we shall call "initial current" value. At longer times, the transient current decays from the initial current value if traps are present.

Before the irradiation, the initial current density-voltage characteristics J(V) agree quantitatively with the theory of trap-free space-charge-limited current in solids. We obtain for the electron mobility a temperature dependence which indicates that scattering due to impurities is weak. This is expected for the high purity silicon used. The drift velocity-field relationships for electrons at room temperature and 77°K, derived from the initial current density-voltage characteristics, are shown to fit the relationships obtained with other methods by other workers. The transient current response for $t > 0$ remains practically constant at the initial value, thus indicating negligible trapping.

Measurement of the initial (trap-free) current density-voltage characteristics after the irradiation indicates that the drift

velocity-field relationship of electrons in silicon is affected by the radiation only at low temperature in the low field range. The effect is not sufficiently pronounced to be readily analyzed and no formal description of it is offered. In the transient response after irradiation for $t > 0$, the current decays from its initial value, thus revealing the presence of traps. To study these traps, in addition to transient measurements, the DC current characteristics were measured and shown to follow the theory of trap-dominated space-charge-limited current in solids. This theory was applied to a model consisting of two discrete levels in the forbidden band gap. Calculations and experiments agreed and the capture cross-sections of the trapping levels were obtained. This is the first experimental case known to us through which the flow of space-charge-limited current is so simply representable.

These results demonstrate the sensitivity of space-charge-limited current flow as a tool to detect traps and changes in the drift velocity-field relationship of carriers caused by radiation. They also establish that devices based on the mode of space-charge-limited current flow will be affected considerably by any type of radiation capable of introducing traps. This point has generally been overlooked so far, but is obviously quite significant.

LIST OF SYMBOLS

Symbols	Meaning	Page Symbol First Appears
J_{sc}	Trap-free space-charge-limited current density.	2
ε	Dielectric constant of silicon.	2
$v(E)$	Drift velocity-field relationship of electrons in Si.	2
V	Voltage across the device.	2
W	Thickness of the device.	2
μ	Electron mobility in silicon.	2
v_s	Limiting drift velocity of electrons in silicon.	2
n_o	Free carrier concentration in the silicon at thermal equilibrium.	3
J_Ω	Current density in the Ohmic range of the device characteristic.	3
q	Value of the electronic charge.	3
V_{TFL}	Trap-filled-limit voltage.	5
θ	Ratio of the free to the trapped carrier concentrations.	5
N_c	Density of states in the conduction band.	5
N_t	Concentration of traps.	5
E_t	Energy depth of the trap below the conduction band.	5

Symbols, Cont'd.

J_{sct}	Shallow trap-dominated space-charge-limited current density.	6
t_o	Transit time of electrons in the device for a uniform electric field.	8
τ'	Trapping time constant.	8
τ''	Detrapping time constant.	8
σ	Capture cross-section of the trap.	8
v_{th}	Thermal velocity of the electrons.	8
N_A	Concentration of acceptors.	14
N_D	Concentration of donors.	14
ϕ	Dose of fast neutrons per cm^2.	32
E_{fo}	Position of the fermi level below the conduction band at thermal equilibrium.	38
E_{f1}	Position of the fermi level at the transition between the Ohmic range and the trap-free space-charge-limited range.	40
V_1	Value of the voltage at the transition between the Ohmic range and the trap-free space-charge-limited range.	40
E_{f2}	Position of the fermi level at the transition between the Ohmic range and the trap-dominated space-charge-limited range.	41

Symbols, Cont'd.

V_2	Value of the voltage at the transition between the Ohmic range and the trap-dominated space-charge-limited range.	41
Subscript f	Refers to the shallower f-level.	46
Subscript s	Refers to the deeper s-level.	46
Subscript x	Refers to the traffic between the f- and s-level.	46
r	Ratio of the maximum amplitude of the fast exponential to that of the slow exponential.	46
J_1, J_2, J_{off}	See Fig. 23.	
n	Carrier concentration in the conduction band.	76
N	Total concentration of injected carriers at the applied voltage v_a.	76

TABLE OF CONTENTS

INTRODUCTION

As Lampert, Rose and Smith pointed out[1], space-charge-limited current can be used to study imperfections in solids. Through the manipulation of a single type of carrier, namely through the voltage controlled injection of excess carriers of one sign of charge, all localized states in the forbidden band gap can be seen in the characteristics of space-charge-limited current under steady state conditions. Steady state measurements will yield information like the concentrations and the energy depths of the levels. Further information, like the capture cross-sections can be obtained with transient measurements.

In previous applications of this technique, for example to CdS[2], the imperfections existed in the crystal ab initio. In this work, the technique has been applied for the first time to the same crystal, before and after the imperfections are introduced. This is possible because of the near perfect condition of the original silicon single crystal. In this instance, the imperfections are introduced by 14 MeV neutron radiation. The comparison of measurements before and after irradiation show conclusively how the imperfections introduced alter the current flow. The theory of space-charge-limited current is applied and a simple model of localized levels in the forbidden band gap is obtained.

The emphasis of this work is on the space-charge-limited current flow i.e. in the range of high applied voltage. Some data in the low voltage range are obtained as well, but these results are peripheral in the present context. They have resisted simple explanation so far.

CHAPTER I

REVIEW OF SINGLE CARRIER SPACE-CHARGE-LIMITED CURRENT

1.1 Steady state trap-free space-charge-limited current.

For a perfect insulator of length W with an injecting contact at x = 0, single carrier space-charge-limited current (sclc) is given by the two equations[3]

$$J_{sc} = \varepsilon \int_0^{E(x)} \frac{v(E)}{x}\, dE, \tag{1a}$$

$$V = \int_0^W E(x)\, dx \tag{1b}$$

where v(E) is the drift velocity-field relationship of the carrier in the material, ε is the dielectric constant of the material and V is the value of the applied voltage. At low electric fields in silicon $v = \mu E$, where μ is the mobility, Eqs. (1) reduce to

$$J_{sc} = (9/8)\varepsilon\mu V^2/W^3 \tag{2}$$

At high electric fields in silicon, the drift velocity of electrons reaches a limiting value $v = v_s$; Eqs. (1) then give

$$J_{sc} = 2\varepsilon v_s V/W^2. \tag{3}$$

In the region of transition between Eqs. (2) and (3), Eqs. (1) can be

solved analytically or numerically when the dependence v(E) is known. On the other hand, the drift velocity-field relationship v(E) can be derived numerically by an inversion of the system of Eqs. (1) if J(V) is known[4]. In our analysis of sclc, we shall use various empirical equations for v(E) from which theoretical J(V) characteristics can be obtained and fitted to experimental sclc data. This procedure is fast and its accuracy is adequate.

If, at thermal equilibrium, the material is such that a nonvanishing concentration n_o of free carriers is present, the DC characteristic can display an Ohmic region at low operating points[5]. Such a case is shown in Fig. 1. This J(V) characteristic is typical of the $n^+ \nu n^+$ structure used in this work. At low voltages the current is Ohmic; the device behaves as a resistor. At higher voltages, the current is space-charge-limited and is proportional to V^2. There is a transition region between the Ohmic and the V^2 range. Marsh and Viswanathan[6] have shown that the square law component of the sclc can be extracted from this transition region by expanding the general solution for the current density J as

$$J \cong (9/8)\varepsilon\mu V^2/W^3 + (3/4)q\mu n_o V/W + (13/360)q^2 n_o^2 \mu W/\varepsilon \qquad (4)$$

$$J \cong J_{sc} + (3/4)\, J_{\Omega} + J_k$$

where q is the value of the electronic charge. Except for the component J_{sc}, all these currents are experimentally accessible

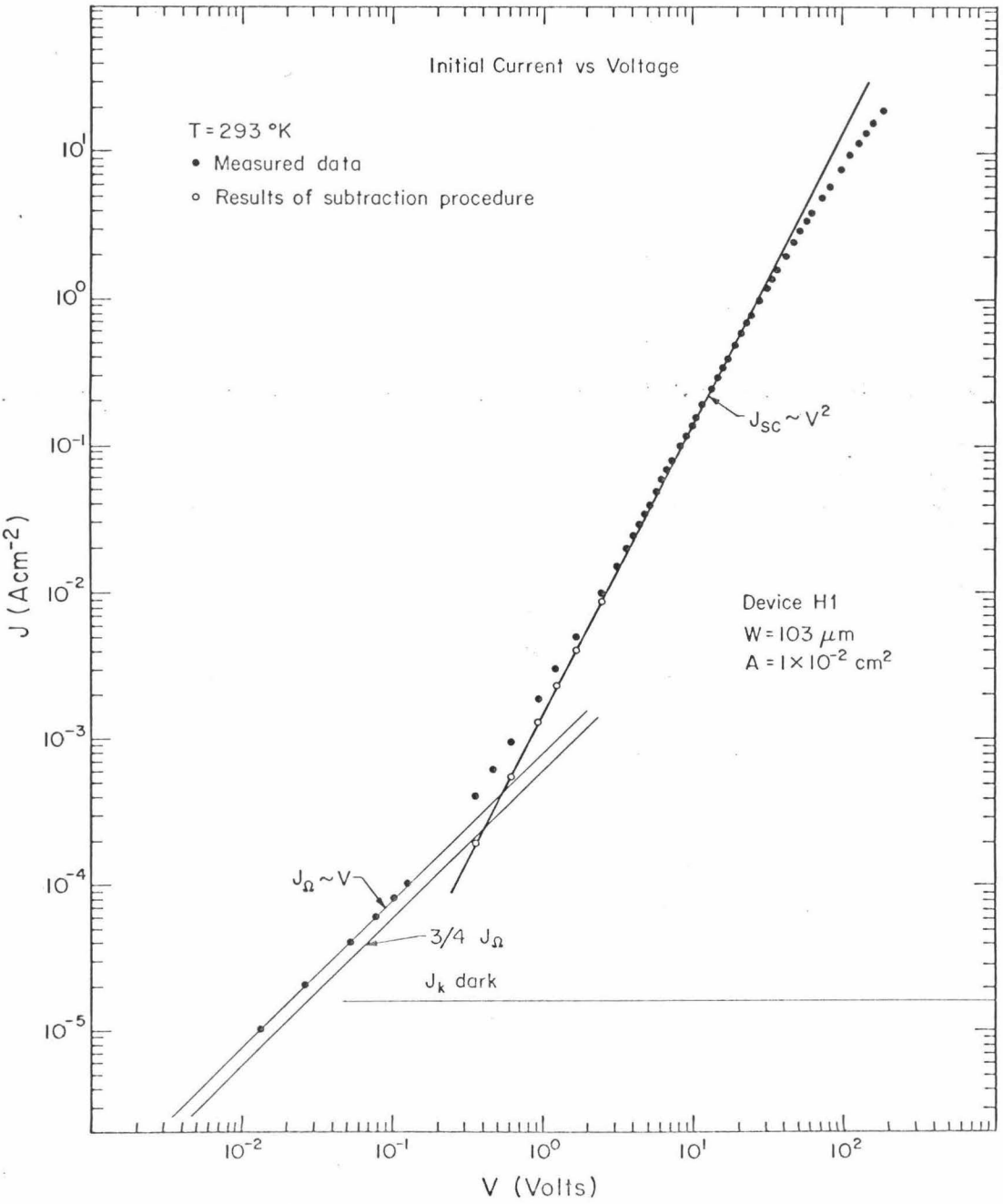

Figure 1 Typical characteristic of initial current density vs voltage before irradiation showing Ohmic and space-charge-limited ranges. The square law asymptote is determined by the subtraction procedure.

quantities. By subtracting J_k and 3/4 of the Ohmic current component J_Ω from the measured value J, one finds J_{sc} (see Fig. 1). This "subtraction procedure" extends sclc in the square law range to low voltages even if a significant Ohmic current component exists.

1.2 Steady state sclc dominated by shallow traps.

The presence of charge carrier traps in the material modifies pure (trap-free) sclc[7,8]. The main features of trap-dominated sclc are: (i) a reduction ("suppression") of the current as compared to trap-free sclc, sometimes by orders of magnitude, because the injected carriers are immobilized in traps, (ii) a steep rise in current at a trap-filled-limit voltage V_{TFL} which occurs when all the traps in the material are being completely filled. This transition from trap-dominated to trap-free sclc occurs over approximately one order of magnitude in voltage and is centered around V_{TFL} for traps distributed uniformly in space and located at a single energy level.

We define θ as the equilibrium ratio of the free to the trapped carriers. For a single shallow trapping level i.e. a level located energetically several kT's above the fermi level, θ is given by Boltzmann's statistics and can be written as

$$\theta = \frac{N_c}{N_t} \exp(-\frac{E_t}{kT}) \qquad (5)$$

where N_c is the effective density of states in the conduction band (for electron trapping), N_t is the concentration of traps and E_t (>0)

is the energy depth of the trap level below the conduction band*. Here, all levels are assumed to have equal statistical weight. In the shallow trap case of interest which we deal with, $\theta << 1$, and, the concentration at thermal equilibrium of carriers on trapping sites is very small compared to $\acute{N}_t$. Then the trap-dominated sclc J_{sct} (for $V << V_{TFL}$) is characterized by

$$J_{sct} = \frac{\theta}{\theta+1} J_{sc}$$

The trap-filled-limit voltage V_{TFL} is related to the concentration N_t by

$$V_{TFL} = \frac{1}{2\varepsilon} qN_t W^2 \qquad (6)$$

An idealized J(V) characteristic of such a situation is shown in Fig. 2. An important point of the shallow trap case is that θ is independent of x except in the narrow region near the emitter[7].

1.3 Transient trap-free and (shallow) trap-dominated sclc.

The theory of transient sclc in the presence of a single shallow trapping level has been developed by Many and Rakavy[9] and Mark and Helfrich[10].

Following a large turn-on voltage step, sclc exhibits a transient

---

*In this work, energies in the forbidden band gap are considered positive and measured from the conduction band edge.

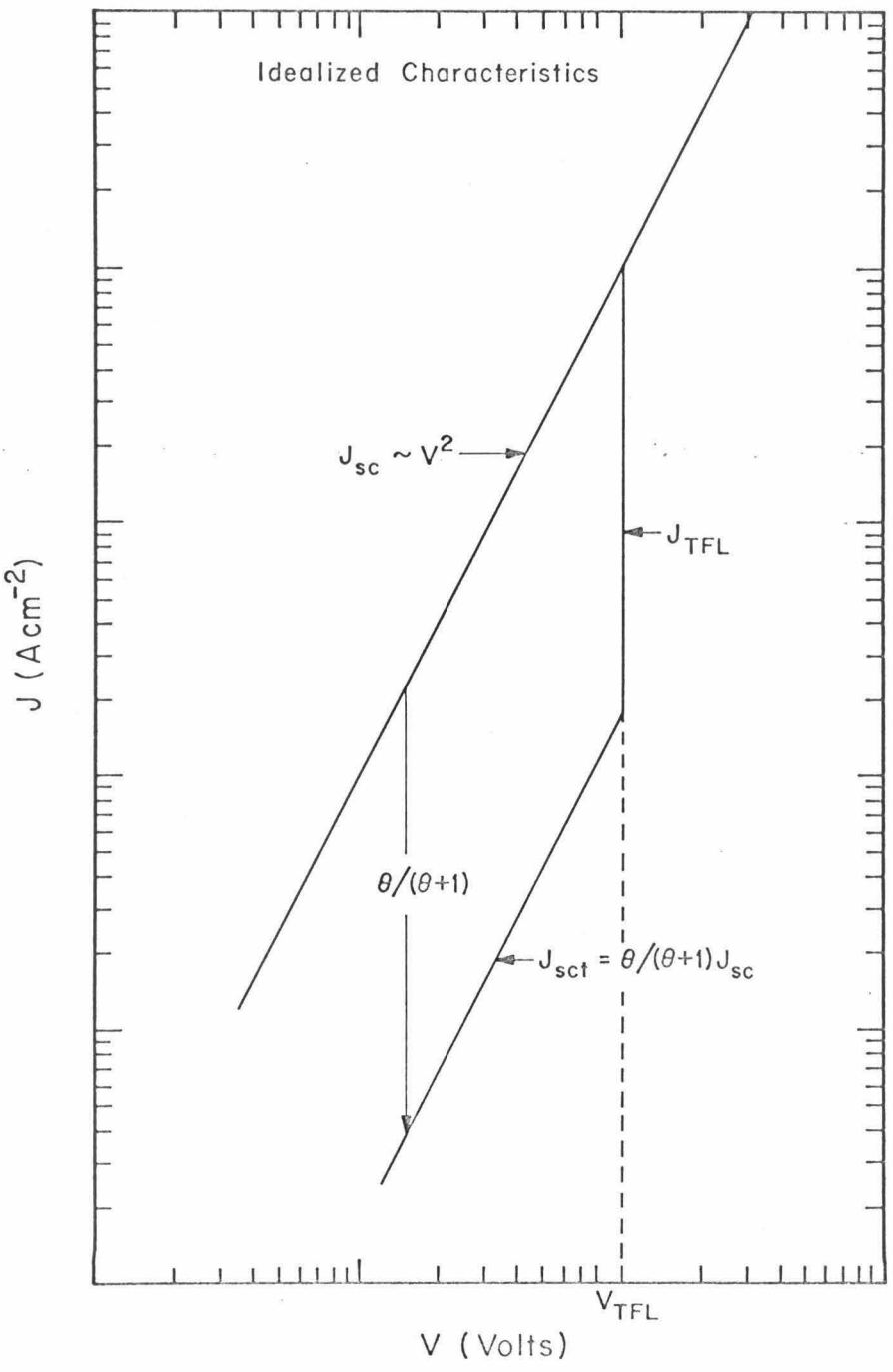

Figure 2 Idealized J(V) characteristics of sclc in the presence of shallow traps.

which lasts for a few t_o, where $t_o = W^2/\mu V$ is the transit time of the charge carriers for a uniform electric field. Subsequent to this transient, sclc will reach a steady state value J_{sc} which we shall call "initial current." Both theory and experiment show that this initial current is unaffected by traps (i.e. trap-free) if the trapping time τ' is large compared to t_o.

As time progresses, however, for an applied voltage $V << V_{TFL}$, the current will decay exponentially with time from its initial current value with a time constant τ_o given by

$$\tau_o = \tau' \ (\theta+1)^{-1} \tag{7}$$

τ' is defined as

$$\tau' = (N_t \ \sigma \ v_{th})^{-1} \tag{8}$$

where σ is the capture cross-section of the traps and v_{th} is the thermal velocity of the carriers.

As shown by Gregory et al[11], the condition $V << V_{TFL}$ ensures that, during the transient, the concentration of carriers in the traps is negligible compared to N_t. With this condition, the current as a function of time t, for t larger than several t_o, is given by

$$J\ (t) = J_{sc} \left(\frac{e^{-t/\tau_o}}{\theta+1} + \frac{\theta}{\theta+1} \right) \tag{9}$$

As we will discuss later (section 3.3), it is possible to determine the detrapping time τ'' from double pulse experiments. τ'' is defined as

$$\tau'' = \frac{1}{P}$$

where P is the probability per unit time that a trapped carrier is released from the traps into the conduction band. Under steady state conditions,

$$\frac{\tau'}{\tau''} = \theta \qquad (10)$$

This follows directly from mass-action considerations.

Therefore, if one determines experimentally τ', τ'' and θ , one has an internal self-consistency check in Eq. (10) above. With N_t determined from the measurement of V_{TFL}, σ and E_t of the traps can then be obtained.

1.4 Sclc in the presence of deep traps.

When the traps are not shallow, the results of sections 1.2 and 1.3 are no longer applicable. In this case, the equilibrium ratio of free to trapped carriers, which is called θ for the shallow trap case, is strongly dependent on x[12]. Because of that x dependence, the problem of deep traps depends on the specific case considered and will be discussed in conjunction with experimental data.

1.5 Summary.

Trap-free sclc yields information on the drift velocity-field relationship of the charge carrier in the material. Sclc dominated by shallow traps yields the trap concentration in the bulk through the

presence of a V_{TFL} and, together with θ, the trap depth E_t. From the time dependence of the current, information on such properties of the traps as the capture cross-section σ can be obtained.

CHAPTER II

MATERIAL EVALUATION, STRUCTURE FABRICATION AND METHOD OF MEASUREMENT

2.1 Material evaluation.

The nominal resistivity of the ν-type silicon ingot used in this work is 75,000Ωcm according to the manufacturers' specifications. The main impurity is phosphorous compensated by boron, as communicated by the manufacturers.

2.1.1 Capacitance measurements.

Schottky barrier capacitance measurements are made at room temperature in the dark. Gold barriers (typical area = 0.02 cm^2) with guard rings are evaporated on a millimeter thick, polished slice cut perpendicular to the $\langle 111 \rangle$ direction. From the slope of $1/C^2$ vs reverse bias voltage for barriers deposited at different spots of the slice, the average carrier concentration at those spots is obtained (see Table I). The results indicate variation in concentration by factors of around 2 across the slice. The carrier concentration at the center of the slice is systematically higher than the carrier concentration at the periphery. Further, changes in the slope of $1/C^2$ vs V plot for each barrier indicate variations in the carrier concentration of the same order along the $\langle 111 \rangle$ axis (see Fig. 3).

TABLE I

Results of Schottky Barrier Capacitance Measurements

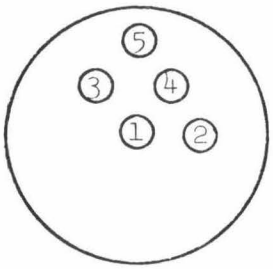

Barrier No.	Carrier conc. n_o (cm^{-3})	Resistivity (kΩcm)
1	2.02×10^{11}	23.0
2	1.53×10^{11}	30.3
3	1.45×10^{11}	32
4	1.61×10^{11}	28.8
5	0.75×10^{11}	61.8

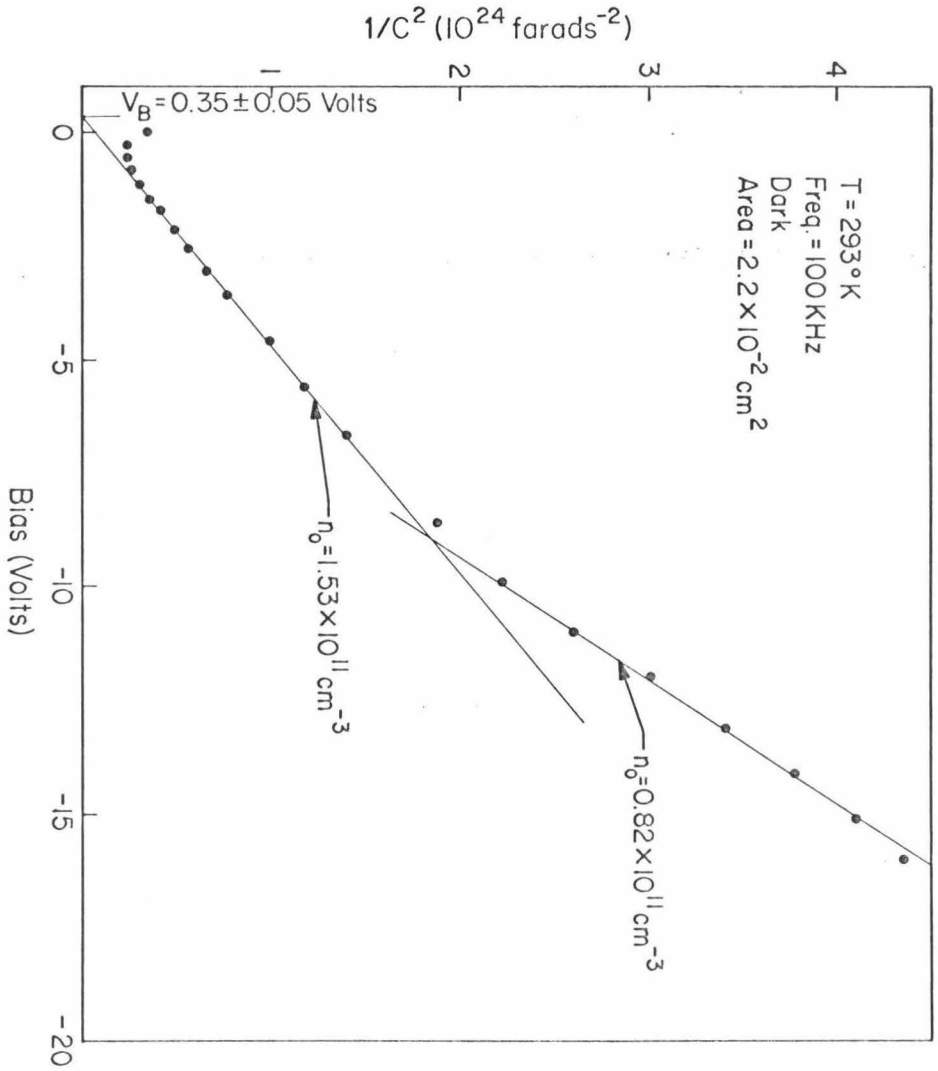

Figure 3 The variation of the free carrier concentration as seen from the plot of $1/C^2$ vs bias voltage of a typical Schottky barrier capacitance measurement.

2.1.2 Four point probe measurements.

Four point probe measurements are made at room temperature on the surface of the ingot exposed after cutting two slices for capacitance and Hall effect measurements. This surface is perpendicular to the $\langle 111 \rangle$ direction and is lapped on 800 mesh carborundum. The distance between adjacent points of the four point probe is 1.28mm. The resistivities obtained as a function of location on the slice are plotted in Fig. 4. We note that the resistivity increases by a factor of around 3 going out radially from the center to the periphery. This increase in the radial direction is in agreement with the observation made from capacitance measurements.

2.1.3 Hall effect measurements.

Two Hall samples are cut from two parts of a slice (see Figure in Table II). Each sample has three pairs of arms labelled from 1 to 3. Data are taken in the dark at $293^{o}K$ and $77^{o}K$. The results are listed in Table II.

We note that arm 2 of Sample II, which comes from the center of the slice yields the highest carrier concentration. Sample I, which comes from the periphery of the slice, yields the lowest carrier concentration. Also, for Sample I and arms 1 and 3 of Sample II, we note that n_o decreases with temperature.

As communicated by the manufacturers, the main donor impurity is P and the main acceptor impurity is B. With a net free carrier concentration of around 10^{11} cm^{-3}, there is negligible "freezing in" of the donors at $77^{o}K$ unless N_A and N_D are of the order of 10^{14} cm^{-3} or higher.

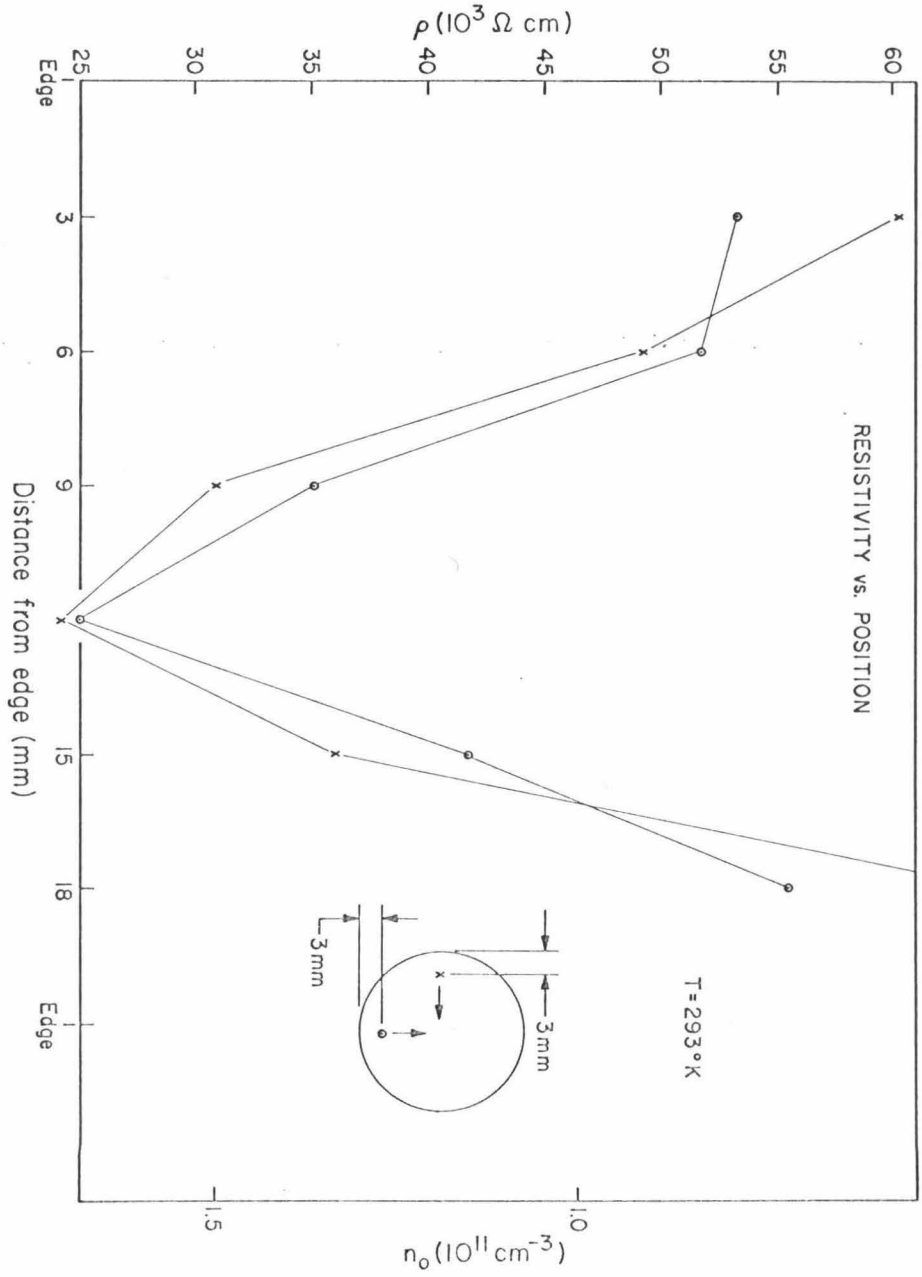

Figure 4 Resistivity as determined from four point probe measurements vs position along two diameters of a (111) surface of the silicon ingot.

TABLE II

Results of Hall Effect Measurements

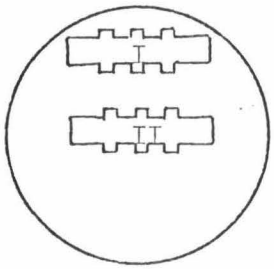

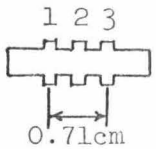

	carrier conc. n_o (cm^{-3})	
	$T = 293^oK$	$T = 77^oK$
Sample I - All arms	1.1×10^{11}	0.52×10^{11}
Sample II - arms 1 & 3	1.85×10^{11}	1.25×10^{11}
Sample II - arm 2	2.7×10^{11}	2.7×10^{11}

But N_D and N_A cannot be much larger than $\sim 10^{13}$ cm^{-3} without creating p-type regions due to random fluctuations. Since no p-type regions are observed, we conclude $N_D \sim N_A \sim 10^{13}$ or less. Hence, the decrease in the free-carrier concentration for the high resistivity portion of the ingot (periphery) as a function of temperature must be attributed to deep levels. Further evidence for the presence of these levels is given in Appendix 2.

To summarize, from capacitance, four point probe and Hall effect measurements, we obtain a consistent picture of the crystal used in this work. The carrier concentration is of the order of 10^{11} cm^{-3}. It is a factor of 2 or 3 lower at the center than at the periphery.

2.2 Structure fabrication.

The $n^+ \nu n^+$ devices are fabricated, starting from thin slices cut perpendicular to the $\langle 111 \rangle$ direction. The wafers are lapped with silicon carbide 400, 800, 3200 mesh, then mechanically polished with 1μ alumina. The wafer is then cut into strips. Such a strip is heated in concentrated HNO_3 for a few minutes until the beaker is too hot to be held between the fingers. The strip is let to cool in the HNO_3 for about half an hour. Then, it is removed and etched in 20:1 HNO_3:HF mixture for about two minutes. The mixture has to be stirred smoothly and continuously. At the end of the two minute period, the etchant is quenched with methanol. Care should be taken to swish the etchant (with the silicon strip in it) vigorously while the methanol is added, in order to prevent the appearance of black silicon polyhydride films on the surface of the strip.

The Si strip is then dipped into HF for a few seconds and placed immediately into the vacuum chamber. About 1μ of 0.5% Sb-Au is evaporated at $\sim 10^{-6}$ Torr on both sides consecutively. The metal is equilibrium alloyed at $\sim 390^{\circ}C$ in an inert nitrogen atmosphere. The slice is then broken into small chips of areas typically around 5×10^{-3} cm^2. Actual areas and thicknesses are determined from photographs taken through a high power microscope. Errors are estimated at ±5% for the area and ±3μ for the thickness. Only devices symmetrical with respect to an inversion of the applied voltage are retained.*

2.3 Measurement circuit and apparatus - measurement procedure.

The circuit used in the pulse measurements is shown in Fig. 5. The overall system has a time resolution of approximately 25 ns.

The electrical measurements are taken between $293^{\circ}K$ and $77^{\circ}K$ ambient temperature. For measurements at $77^{\circ}K$, the sample holder is immersed in liquid nitrogen in a light tight chamber. For higher temperatures, a thermostat is used[13]. To assure standard initial conditions, the device is short-circuited and illuminated with white light prior to each pulse. Care is always taken to wait long enough for thermal equilibrium to be re-established after the white light is turned off. Current is observed with a 454 Tektronix oscilloscope across the 50Ω resistor in series with the device.

Various conditions of ambient illumination are generated in the light tight measuring chamber with light bulbs rated 500mW, bare for "white" illumination or placed in Si and Ge containers with ∿1.5mm

*The yield is roughly 30%.

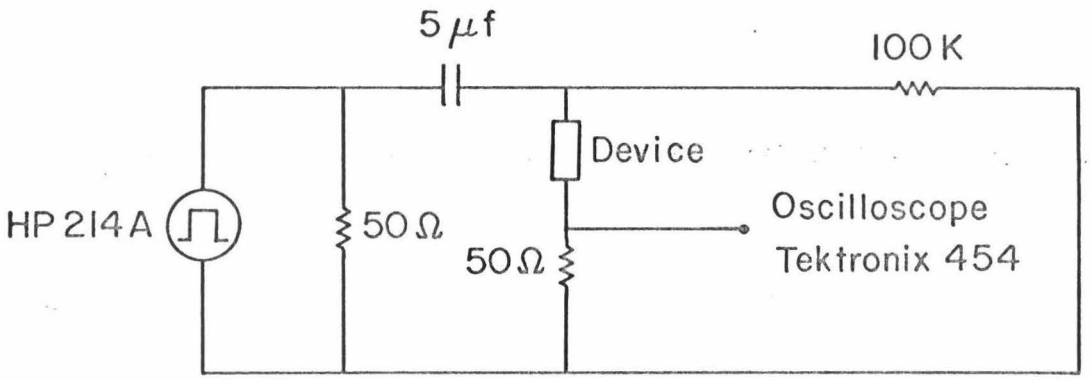

Figure 5 Circuit diagram of the electronic system used for the pulse measurements.

thick walls acting as filters for "Si light" and "Ge light."

For pulse measurements, large and fast (~15 ns rise-time) turn-on voltage pulses about 10-100μs long from a HP 214A generator, are applied in single shots or slow repetition rates. The smallest voltage value still accurately detectable by the oscilloscope is 0.5mV across 50Ω which corresponds to 10 μA. Hence in many samples, the Ohmic range is accessible only with DC measurements.

The DC measurements are obtained using a battery across a potentiometer. Voltage and current are measured using a Keithley electrometer.

2.4 Irradiation procedures.

For the irradiation, the samples are kept in an aluminum container. This container is taped on the back of the water-cooled tritium target of a Texas Nuclear Corporation accelerator at the California State College--Los Angeles. The dose from the d-t reaction is calculated, from the activation analysis of Al foils covered with Cd, by J. L. Shapiro of the California Institute of Technology. Mg and Ni foils are also used for cross checks. The estimated error in the resulting number of fast neutrons per cm^2 is about 10%.

Samples of various thicknesses have been exposed to a dose of 1.2×10^{11} n/cm^2. A few other samples have been irradiated at an initial dose of 5.5×10^{11} n/cm^2 and re-exposed up to a total of 4.0×10^{12} n/cm^2. Unless stated otherwise, the results presented in chapter III refer to the irradiation at a dose of 1.2×10^{11} n/cm^2.

CHAPTER III

RESULTS AND DISCUSSIONS

3.1 Pre-irradiation analysis of the $n^+\nu n^+$ structures.

3.1.1 Trap-free space-charge-limited range.

Typical dependences of the initial current density vs voltage for unirradiated samples are shown in Fig. 6. One observes an Ohmic range, a square law range with some deviation at higher voltages indicating hot carrier effects and, especially at 77^oK, a voltage dependence indicative of velocity saturation[14]. The square law range can be extended to lower voltages and located uniquely by applying the subtraction procedure outlined in section 1.1.

The room temperature data are compared to a theoretical characteristic J(V) computed with a v(E) of the form[3]

$$v = \mu E_o [1 - \exp(-E/E_o)]$$

where μ is the low field mobility and E_o is a constant. This empirical drift velocity-field relationship agrees quite well with the measured drift velocities of electrons in Si at room temperature (Fig. 7)[15]. As indicated in Fig. 6, the theoretical J(V) characteristic fits the pre-irradiation data well. The three related asymptotes of J_Ω and of J_{sc} in the square law regime (Eq. 2 section 1.1) and the linear regime (Eq. 3 section 1.1) of the fit are shown also. In Fig. 8 the current of the square law asymptote (representing Eq. 2 section 1.1) at a

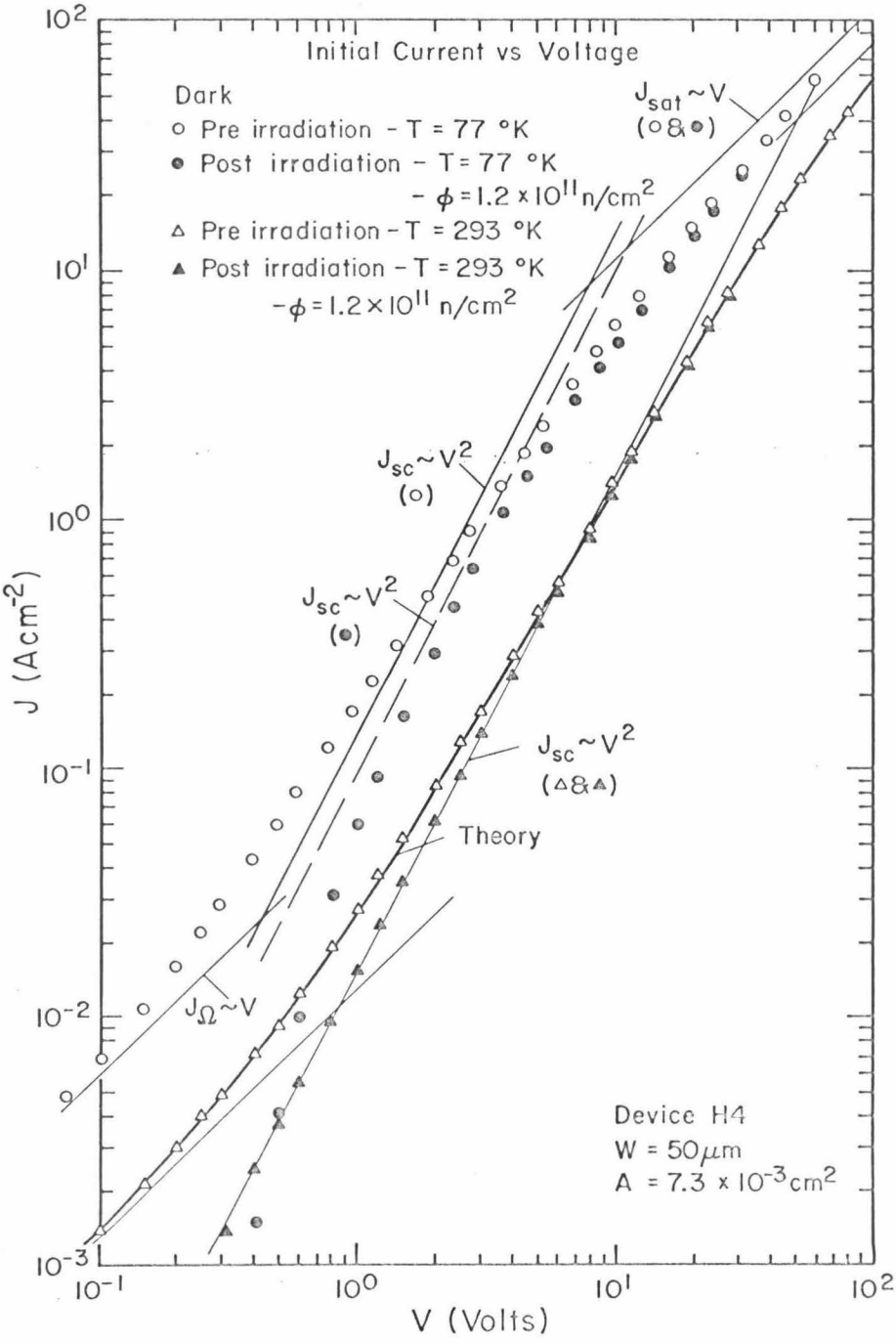

Figure 6 Typical trap-free characteristics of initial current vs voltage before and after irradiation at a dose of $\phi \simeq 1.2 \times 10^{11} n/cm^2$. The solid curve at T = 293°K is the theoretical characteristic obtained using the empirical equation $v = \mu E_o [1-\exp(-E/E_o)]$. The solid lines are the asymptotes of the characteristics before irradiation. The dashed line is the asymptote of the square law range at 77°K after irradiation.

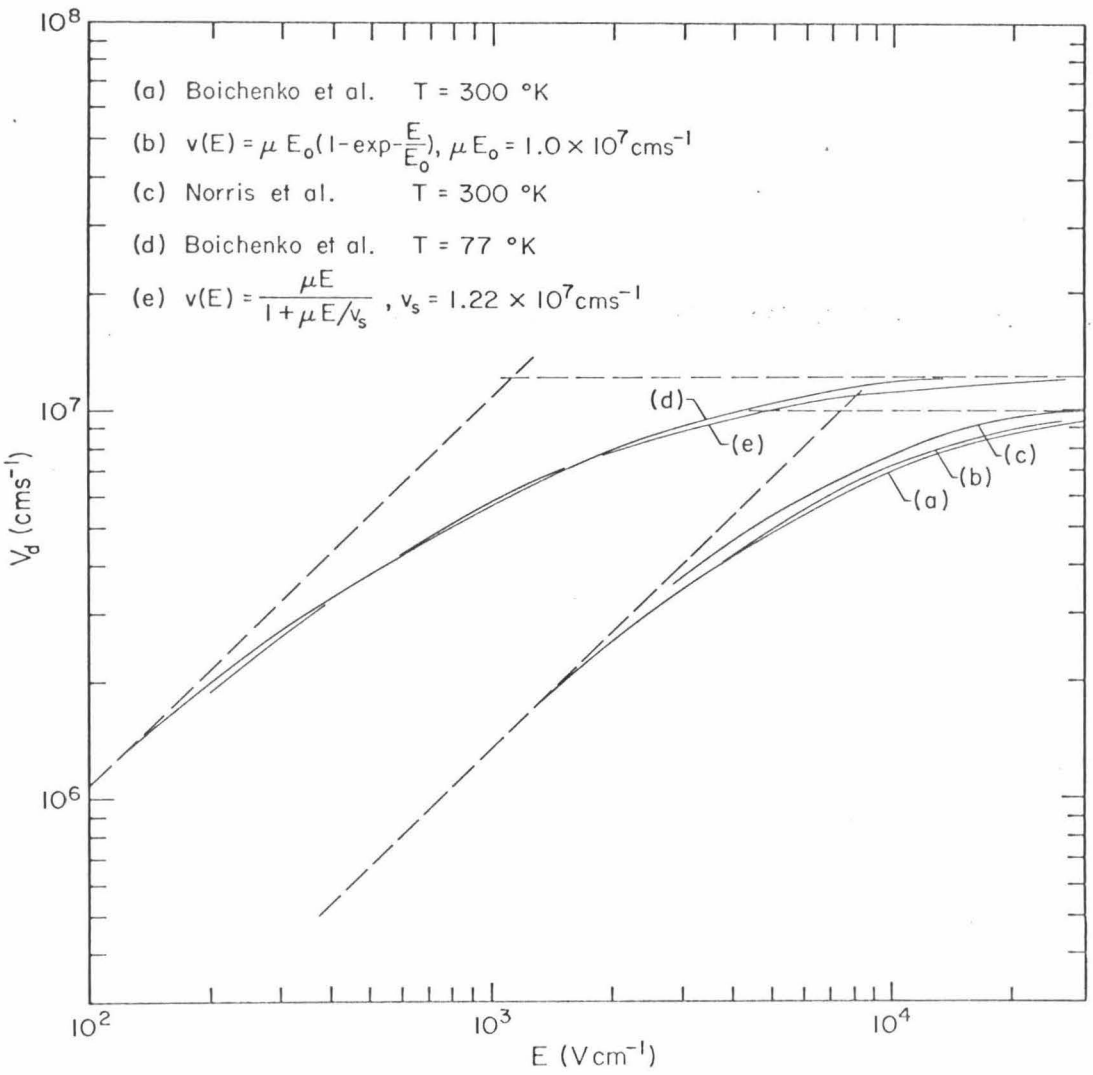

Figure 7 Comparison between experimental drift velocity-field relationships v(E) and the empirical relations used in the analyses of the pre-irradiation characteristics.

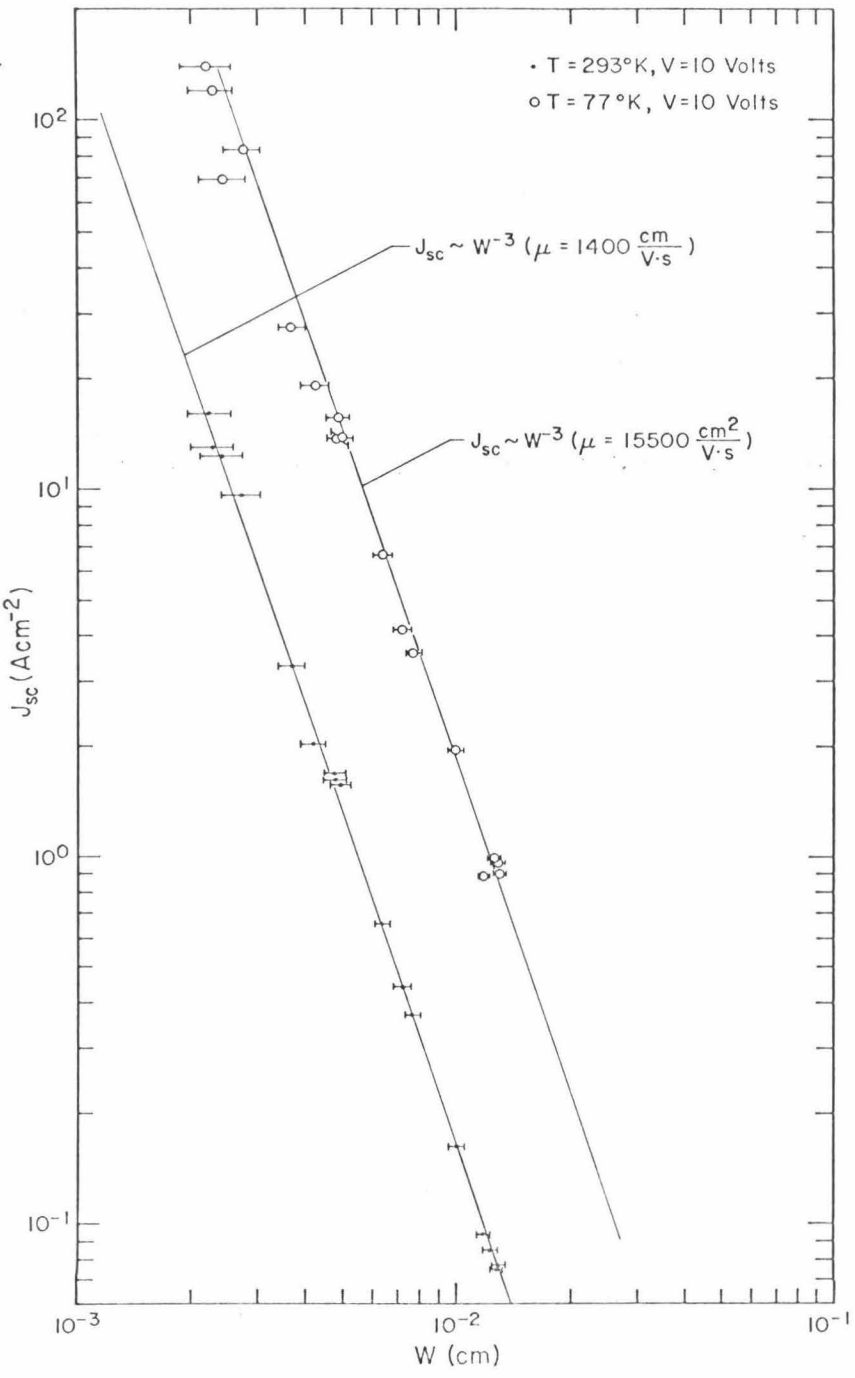

Figure 8 The dependence upon the thickness W of the initial current at a constant voltage of 10 V, derived from the square law asymptotes to the characteristics of a number of devices. The exact position of the asymptotes is established by the subtraction procedure.

constant voltage of 10V and 293°K is plotted for a number of samples as a function of their thickness W. The W^{-3} dependence is accurately confirmed. A mobility value of $\mu = 1400 \pm 50 cm^2/Vs$ is derived from this plot in excellent agreement with accepted values. Corresponding results derived from the high current asymptote (representing Eq. 3 section 1.1) are plotted in Fig. 9, showing the W^{-2} dependence, as predicted by the theory. The value of the limiting drift velocity obtained from this plot is $v_s = (9.6 \pm 1.0)10^6 cm/s$. This is in good agreement with published values[15].

Similar analyses are performed at 77°K (Figs. 8 and 9). At this temperature, a v(E) of the form[16]

$$v = \mu E/(1+\mu E/v_s) \qquad (6)$$

is used to calculate a theoretical J(V). This empirical equation also describes the experimental data available on v(E) very well, as shown in Fig. 7[17]. Again, the theoretical J(V) fits the experimental points well. From the comparison we find $\mu = 15500 \pm 1500 cm^2/Vs$ and $v_s = (12.6 \pm 1.0)10^6 cm/s$. This value of the mobility is approximately one-half that in undoped silicon[18] and suggests the presence of some impurity scattering; that of the limiting drift velocity is again in good agreement with published results[14, 19].

The characteristics of initial current density vs voltage in the temperature $77°K < T < 293°K$ are shown in Fig. 10. We observed in all of them an Ohmic range followed by a square law range with some devia-

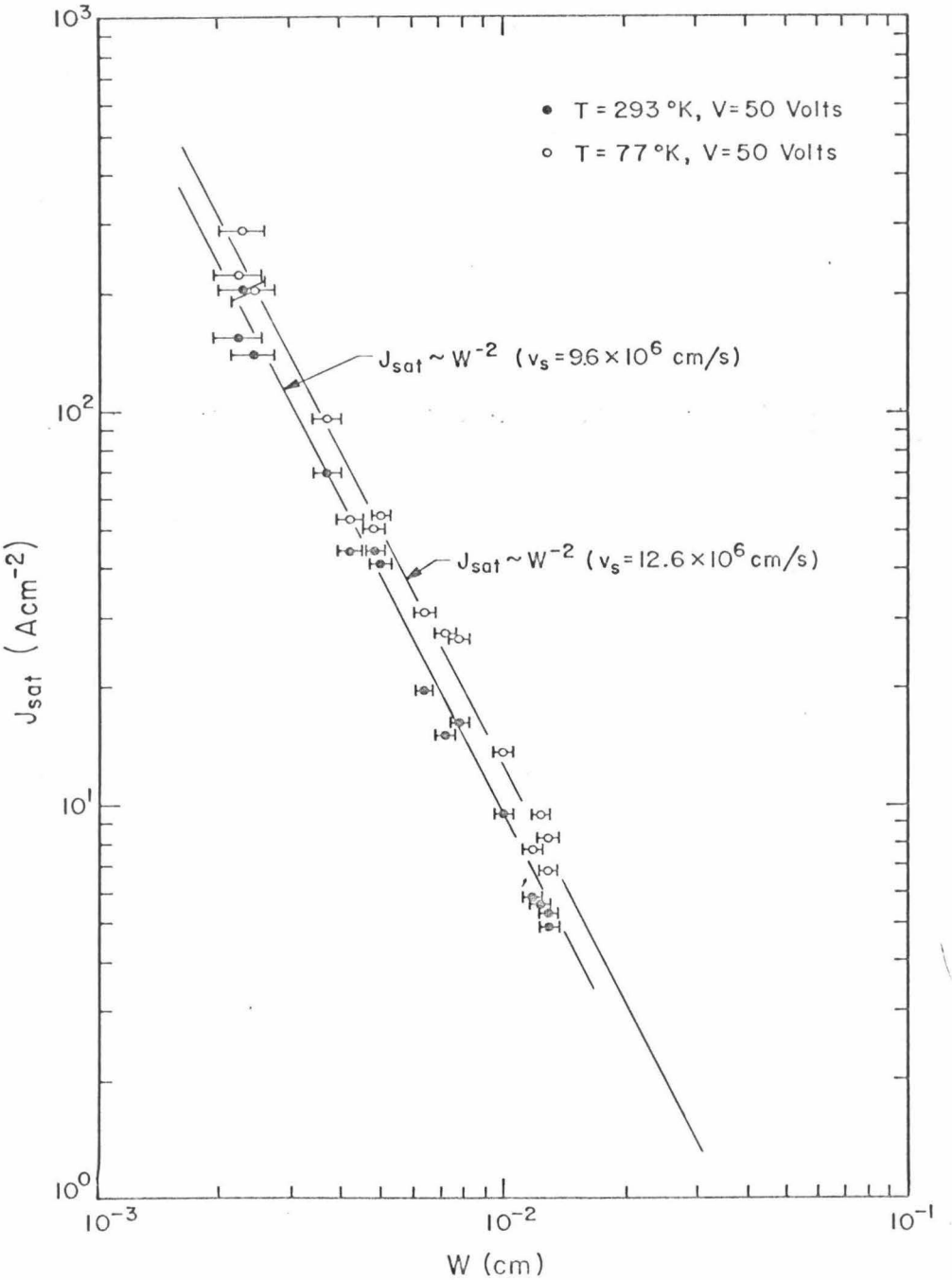

Figure 9 The dependence upon the thickness W of the initial current, at a constant voltage of 50 V, derived from the linear high voltage asymptotes to the characteristics of a number of devices. The position of the high voltage asymptotes is established by matching a theoretical J(V) characteristic to the high voltage portion of the experimental characteristics while keeping the square law asymptotes of the theoretical curve in coincidence with that of the experimental curve, the latter established by the subtraction procedure.

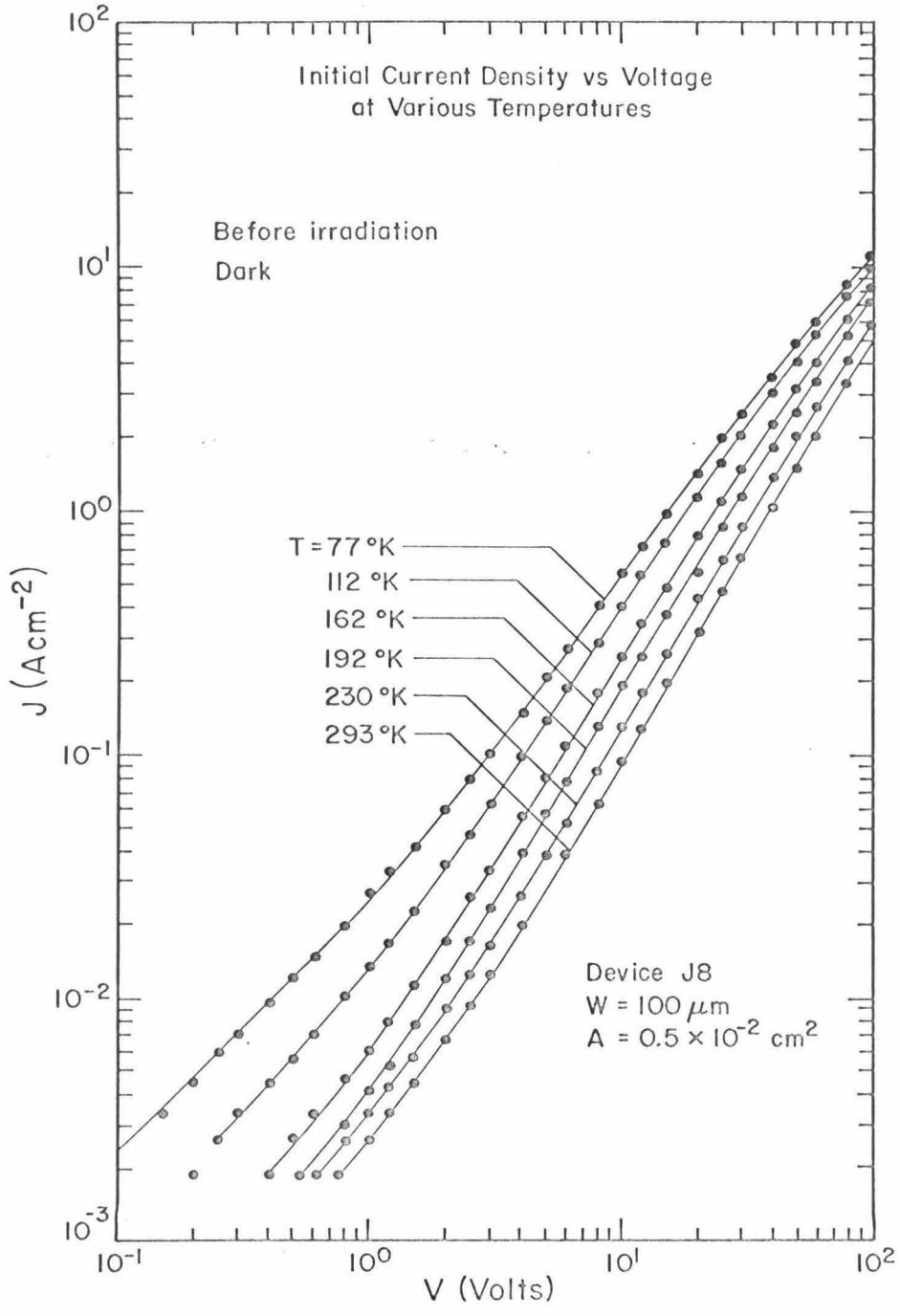

Figure 10 Typical characteristics of initial current vs voltage before irradiation as a function of temperature.

tion indicating hot carrier effects. They lie between the characteristic at room temperature and that at $77^{o}K$ which we have shown to be those of trap-free space-charge-limited current. This suggests that the characteristics in this temperature range are also those of trap-free space-charge-limited current. In Appendix 2, it is shown that, before irradiation, slight trapping is observed in some devices in the sclc range, but the current diminishes only little below its initial value at $t \simeq 0$ (when the voltage pulse is applied). Here, it suffices to note that, relative to the behavior of the devices after irradiation, trapping effects on unirradiated samples are negligible in the sclc range. In Fig. 11, the current of the square law asymptote at a constant voltage of 10V is plotted as a function of temperature. The dependence is very close to a T^{-2} power. Since μ is the only temperature dependent parameter in Eq. (2), section 1.1, we obtain

$$\mu \propto T^{-2}$$

This dependence indicates that impurity scattering is weak except at the lowest temperatures[18]. This is expected, owing to the high resistivity of the starting material.

In the intermediate temperature range $77^{o}K < T < 293^{o}K$, the data points available are insufficient to compare the dependence of v_s on temperature with that found in the literature[14, 19].

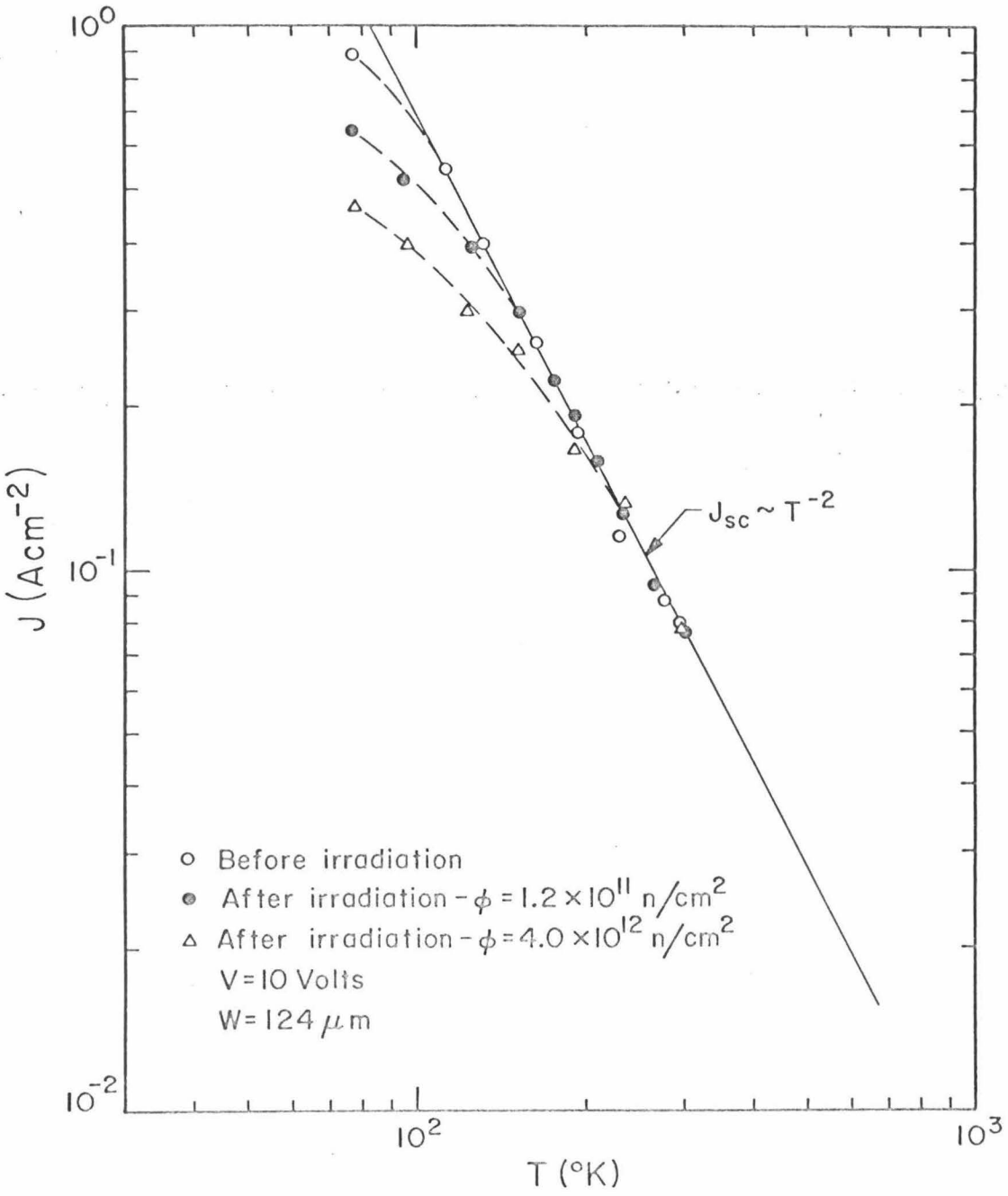

Figure 11 The dependence upon temperature of the initial current, at a constant voltage of 10 V, derived from the square law asymptotes of the device characteristics before and after irradiation at a dose of $\phi \simeq 1.2 \times 10^{11}$n/cm^2 and $\phi \simeq 4.0 \times 10^{12}$n/cm^2.

3.1.2 Summary.

The results presented establish that the initial current flowing through a device immediately after the application of a voltage pulse constitutes trap-free sclc. They are in quantitative agreement with the theory.

3.2 Post-irradiation analyses of the $n^+\nu n^+$ structures.

3.2.1 Trap-free space-charge-limited range; effect on v(E).

Fig. 6 shows typical initial (trap-free) current vs voltage characteristics in the dark before and after irradiation. At 293°K the subtraction procedure applied to the pre-irradiation characteristic yields a sclc component ($J_{sc} \sim V^2$, straight line) which coincides with the post-irradiation characteristic. This result establishes that the effect of fast neutrons on the velocity-field relationship v(E) is negligible for electrons in high purity silicon at 293°K. This is true for doses up to 4.0×10^{12} n/cm^2. At 77°K, we observe a difference between the pre-irradiation and the post-irradiation characteristics. As we will show below, this difference is due to a change in the mobility.

Fig. 12 shows the post-irradiation characteristics of initial current *density* vs voltage as a function of temperature. We observe a space-charge-limited square law behavior followed by a bending over due to hot carrier effects. We notice that a low voltage threshold develops as the temperature decreases. At 77°K, the phenomenon is quite pronounced. The cause of this effect is unclear, but a tentative interpretation is offered in Appendix 2. To find the square law

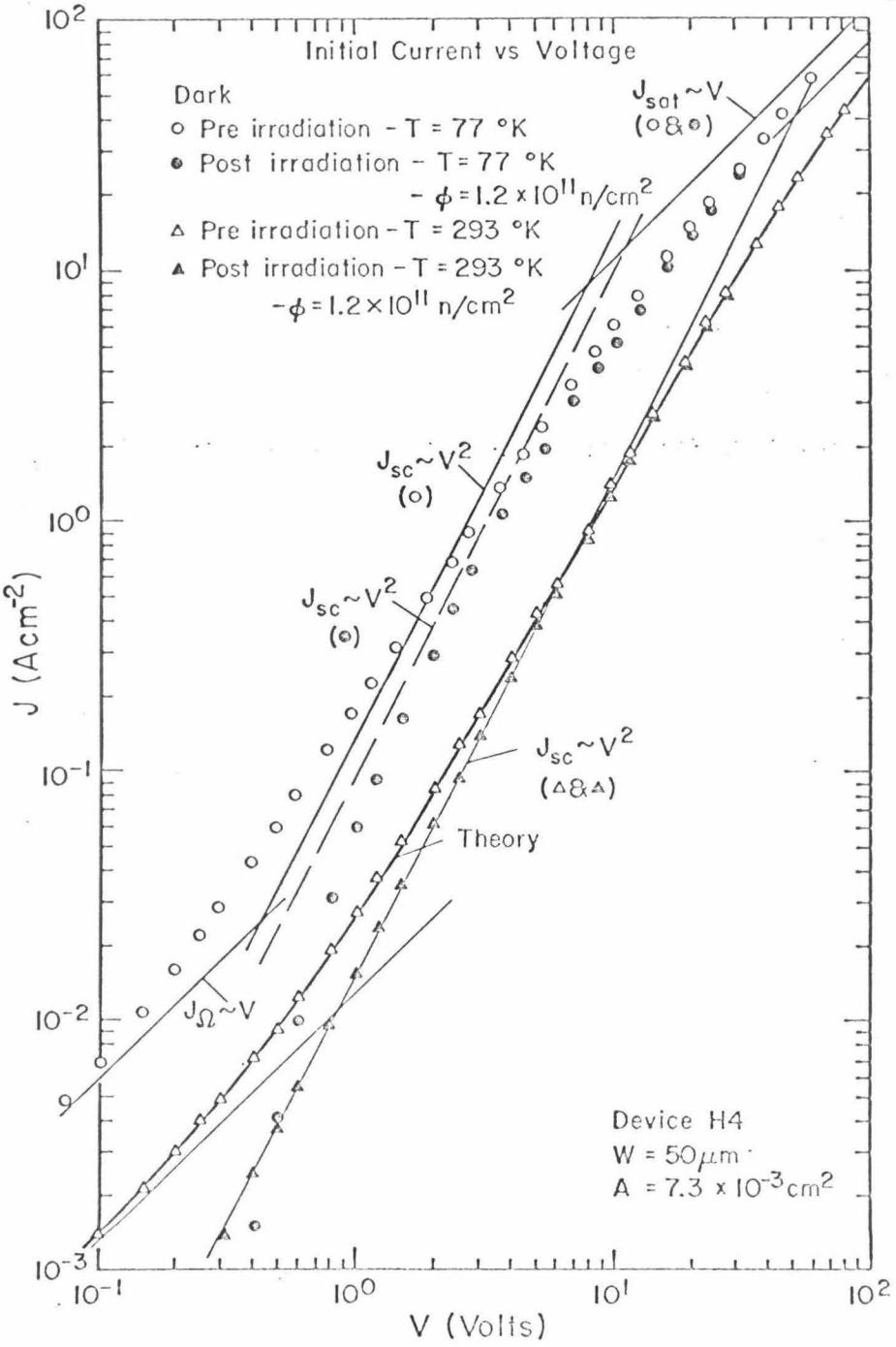

Figure 6 (repeated) Typical trap-free characteristics of initial current vs voltage before and after irradiation at a dose of $\phi = 1.2 \times 10^{11} n/cm^2$. The solid curve at T = 293°K is the theoretical characteristic obtained using the empirical equation $v = \mu E_o [1-\exp(-E/E_o)]$. The solid lines are the asymptotes of the characteristics before irradiation. The dashed line is the asymptote of the square law range at 77°K after irradiation.

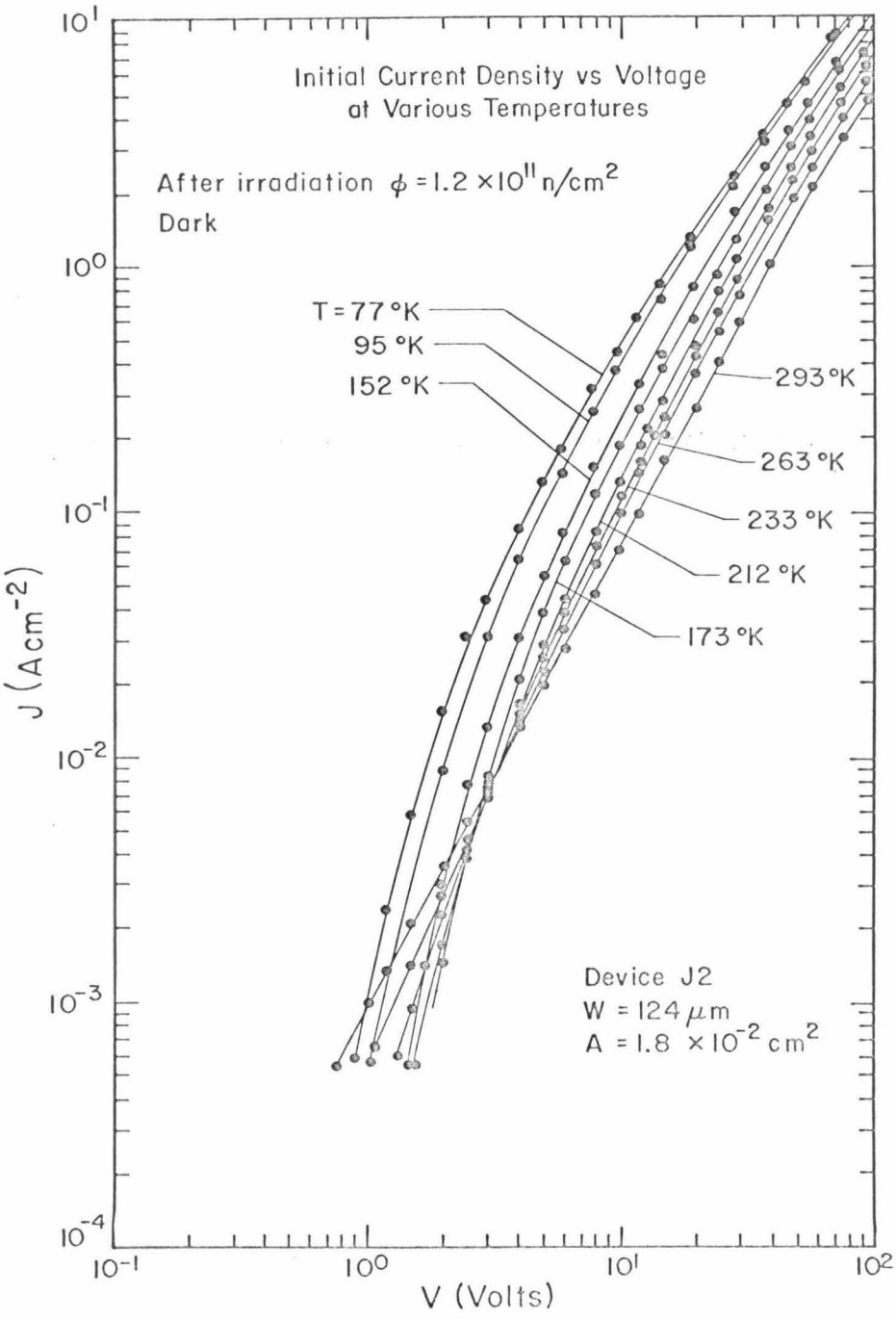

Figure 12 Typical characteristics of initial current vs voltage after irradiation at a dose of $\phi \approx 1.2 \times 10^{11}$ n/cm^2 as a function of temperature showing the "threshold voltage."

asymptote in the sclc range in spite of this complication, two methods are applied: (i) It is assumed that the presence of this threshold leads to an overall characteristic which is very similar to that obtained in devices exhibiting a transition from punch-through to sclc. A theoretical J(V) characteristic of this process, with known position of the square law asymptote, is then fitted to the experimental points.[3] (ii) An Ohmic range is created purposely in the characteristic by illuminating the sample with white light, thus masking the threshold and making the subtraction procedure applicable. Both methods yield the same square law asymptote. The current of these square law asymptotes at a constant voltage of 10V is plotted as a function of temperature in Fig.11. At high temperatures, the dependence is proportional to T^{-2}, identical to the pre-irradiation result. However at temperatures below $T \simeq 140^{o}K$, the values for the dose of $\phi = 1.2 \times 10^{11}$ n/cm^2 drop below those of the pre-irradiation curve. We can therefore conclude that at the dose of $\phi = 1.2 \times 10^{11}$ n/cm^2, the mobility has not changed in the temperature range $140^{o}K < T < 293^{o}K$. Below $T = 140^{o}K$, the mobility is reduced by the irradiation. Within our experimental accuracy, the limiting drift velocity v_s is unaffected by these doses of radiation at all temperatures.

At $77^{o}K$, the mobility value derived shows a decrease from the pre-irradiation value of 15500 cm^2/Vs to 9600 cm^2/Vs (Fig. 6 dashed line). In Fig. 13, we plot the current at $77^{o}K$ of the square law asymptotes at a constant voltage of 10V as a function of thickness W. The W^{-3} dependence is satisfied, confirming that the current is trap

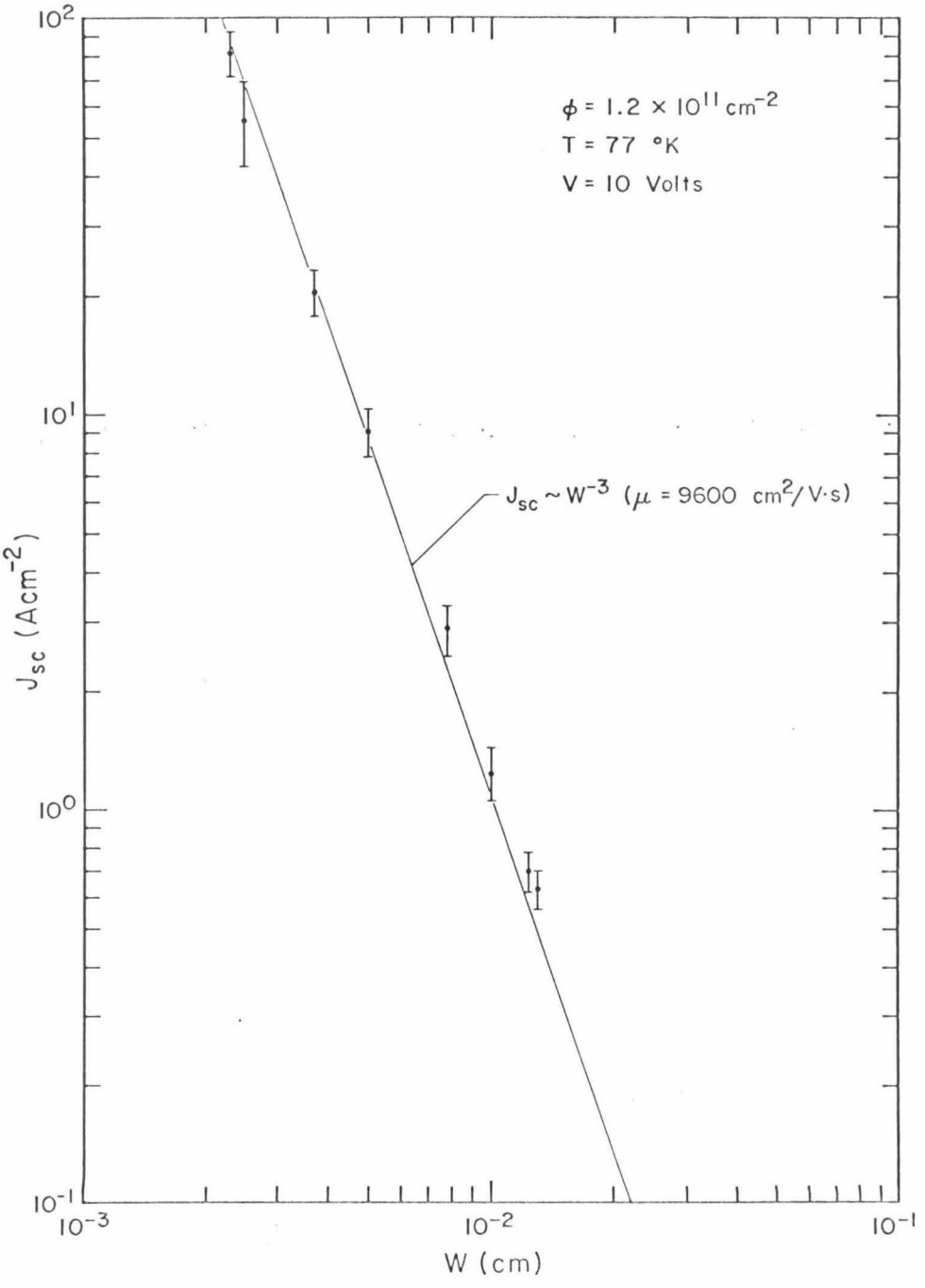

Figure 13 The dependence upon the thickness W of the initial current, at a constant voltage of 10 V, derived from the square law asymptotes of the post irradiation characteristics at 77°K.

free sclc. The value of μ obtained from this plot is $\mu = 9600\ cm^2/Vs$ in agreement with the value derived from Fig. 6. For a dose of $\phi = 4.0 \times 10^{12}\ n/cm^2$, the results on two devices yield $\mu = 7550\ cm^2/Vs \pm 15\%$.

3.2.2 Discussion of effect on v(E).

Up to the dose of $4.0 \times 10^{12}\ n/cm^2$, the only detectable change in v(E) is a reduction of the mobility at low fields and low temperatures. The limiting drift velocity at high fields results from energy losses of the carriers to optical and acoustical phonons. The low doses of this experiment are not expected to alter this process. The mobility at low fields results from scattering with the thermal phonons and with some impurities. Since the number of these phonons decreases with decreasing temperature, additional scattering centers should be noticed first at low temperatures. This agrees with our observation. Unfortunately, the number of data points is too limited to allow a comparison with the Brooks-Herring formula[18]. The results establish, however, that irradiation does indeed introduce additional scattering centers.

In principle, the observed decrease in mobility can also be attributed to very fast trapping with a time constant much smaller than 25ns and, therefore, beyond the resolution of our measurement circuit. This would result in an effective mobility $\mu_{eff} = \mu(\theta/(1+\theta))$, where $\theta/(1+\theta)$ (Section 1.2) is about $(9600/15500) \sim 0.6$ at $77^{\circ}K$ (see Fig. 6). This interpretation requires that the factor $\theta/(1+\theta)$ be exponentially dependent on temperature. Unfortunately again, the data are too limited to allow a check on this dependence. We feel that this interpretation

is quite unlikely.

The accepted model of neutron damage in silicon developed by Gossick[20] invokes defect clusters acting as insulating spheres with dimensions of at least a Debye length. This picture has been derived primarily in conjunction with data obtained at small departures from thermal equilibrium. It is not evident how this model applies, if at all, to conditions of sclc. The large concentration of injected carriers and the strong electric field distributed non-uniformly in the bulk create conditions far different from those of thermal equilibrium. However, if we apply the model in the limit of high carrier concentration, then the radius of each cluster will be reduced to the radius of the actual damaged area which is around 200 Å [20]. In this case, the ratio f of the volume of damaged regions to the total volume, which is given by $f = \frac{v_o \Sigma \phi}{\text{volume}}$ (v_o is the volume of each cluster, Σ is the probability per cm that a fast neutron will produce a cluster $\Sigma \simeq 10^{-1}\,\text{cm}^{-1}$ [21]), will be around 10^{-2} for a typical sample used in this work. Gossick's model predicts the mobility to change as a linear function of f, hence this change would be very small in our case. The same argument can be applied, again with caution, to show that the dielectric constant ε is not affected by the irradiation as we had assumed in the foregoing discussion in which all the change in current density J was attributed to a change in the mobility μ. Indeed, according to Gossick's model, the dielectric constant should increase according to

$$\varepsilon' = \varepsilon \left(\frac{3}{1-f} - 2\right)$$

where ε is the pre-irradiation dielectric constant. With $f \simeq 10^{-2}$, the increase is very small.

More work will be required to study the applicability of the cluster model to conditions of sclc.

3.3 Post-irradiation analysis; trapping phenomena.

Upon the application of a voltage step V_a, the current through our irradiated devices reaches the initial current value, which was analyzed in the preceding chapter, then decays below it (Fig. 14). This decay reveals the presence of traps. In this section 3.3, we shall analyze the results of both DC and transient measurements with the aim of finding the properties of these trapping levels. This procedure yields information about the number of trapping levels, their concentrations, their energy depths below the conduction band, and their capture cross-sections. We will show below that there are two trapping levels which influence the current density-voltage characteristics. For convenience in notation, we will call the shallower level the f-level and the deeper level the s-level. These labels were suggested by the "fast" and "slow" nature of their transient responses at $77^{o}K$. By studying the DC characteristics in the temperature range $200^{o}K < T < 293^{o}K$, information about the deeper s-level is obtained: Its concentration derived from the trap-filled-limit voltage (Eq. 6 Section 1.2), and its energy depth from the factor θ_s (Eq. 5 Section 1.2). The capture cross-section of this s-level is obtained from the room temperature transient measurement of the trapping time (Eq. 8 Section 1.3).

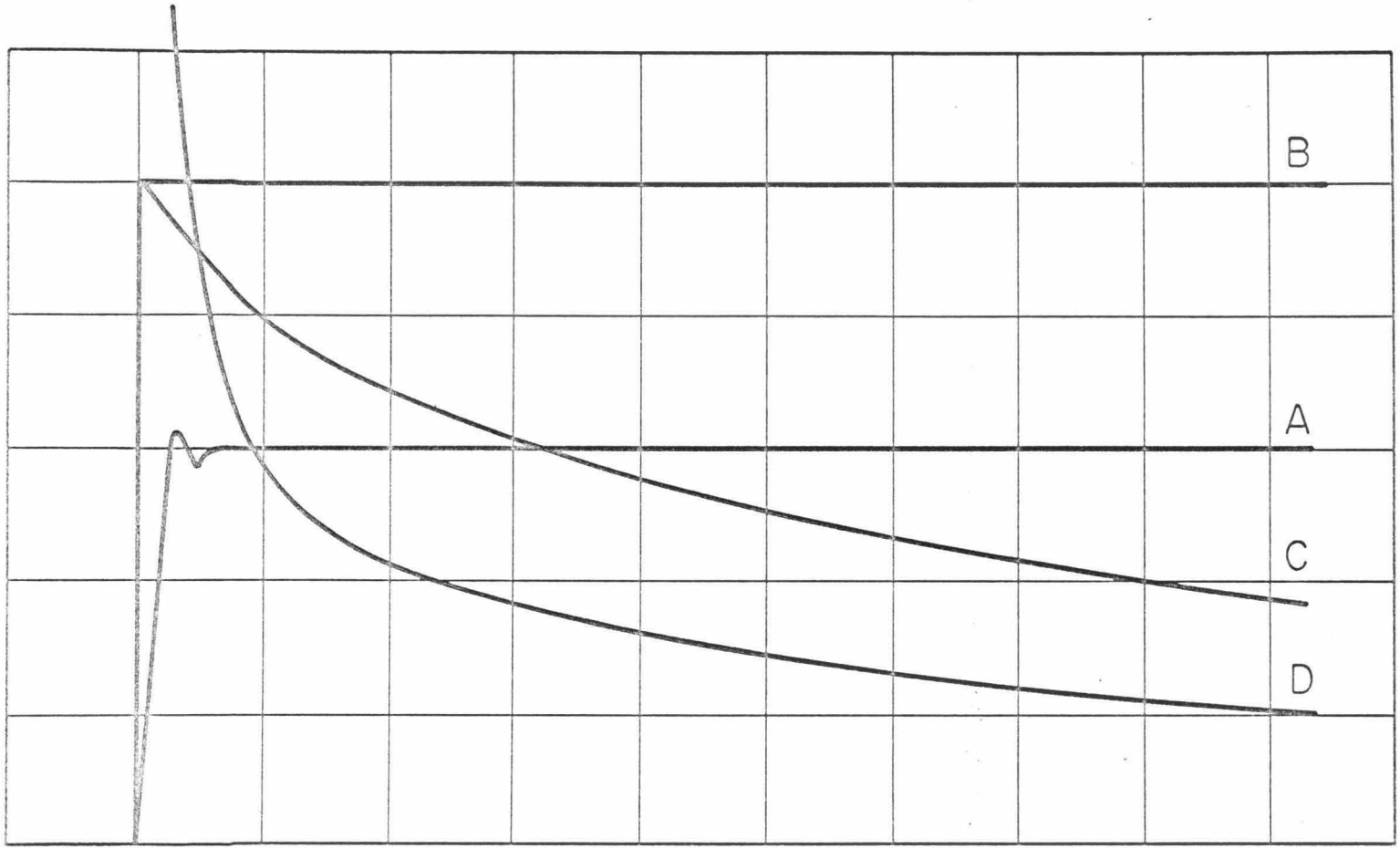

Figure 14 Composite oscillogram of a typical applied voltage pulse and of typical current responses. 1 major division = 1 cm.
A: applied voltage pulse, 5 v/cm vert. and 50 ns/cm horiz.
B: current response before irradiation showing no trapping 20 mA/cm vert. and 1 μs/cm horiz.
C: current response after irradiation showing the fast decay, 4 mA/cm vert. and 1 μs/cm horiz.
D: curve C expanded to show the slow decay, 0.4 mA/cm vert. and 100 μs/cm horiz.

A band model is proposed which explains the observed facts obtained from transient measurements at low temperatures. We obtain the concentration of the shallower f-level from the values of the trap-filled-limit voltage, V_{TFLf}, associated with the f-level, the energy depth from the calculated θ_f using the proposed model, and the capture cross-section from the measured trapping time.

The outline of this section will be as follows:

(1) theoretical discussion of DC characteristics

(2) discussion of experimental DC characteristics

(3) theoretical discussion of proposed band models and their transient responses

(4) discussion of experimental transient measurements

(5) analysis of additional data

(6) summary and discussion.

3.3.1 Theoretical discussion of DC characteristics.

To explain the DC characteristics, the situation represented in Fig. 15 is considered. Let the free carrier concentration at thermal equilibrium in the conduction band be n_o. The corresponding position of the fermi level is at E_{fo}. We assume that E_{fo} is far below the conduction band so that Boltzmann's statistics applies. The transition from a linear Ohmic behavior $J \sim V$ to a space-charge-limited behavior $J \sim V^2$ occurs at the voltage at which the concentration of injected free carriers equals n_o. In other words, the total free carrier concentration n_{free} in the conduction band is given by

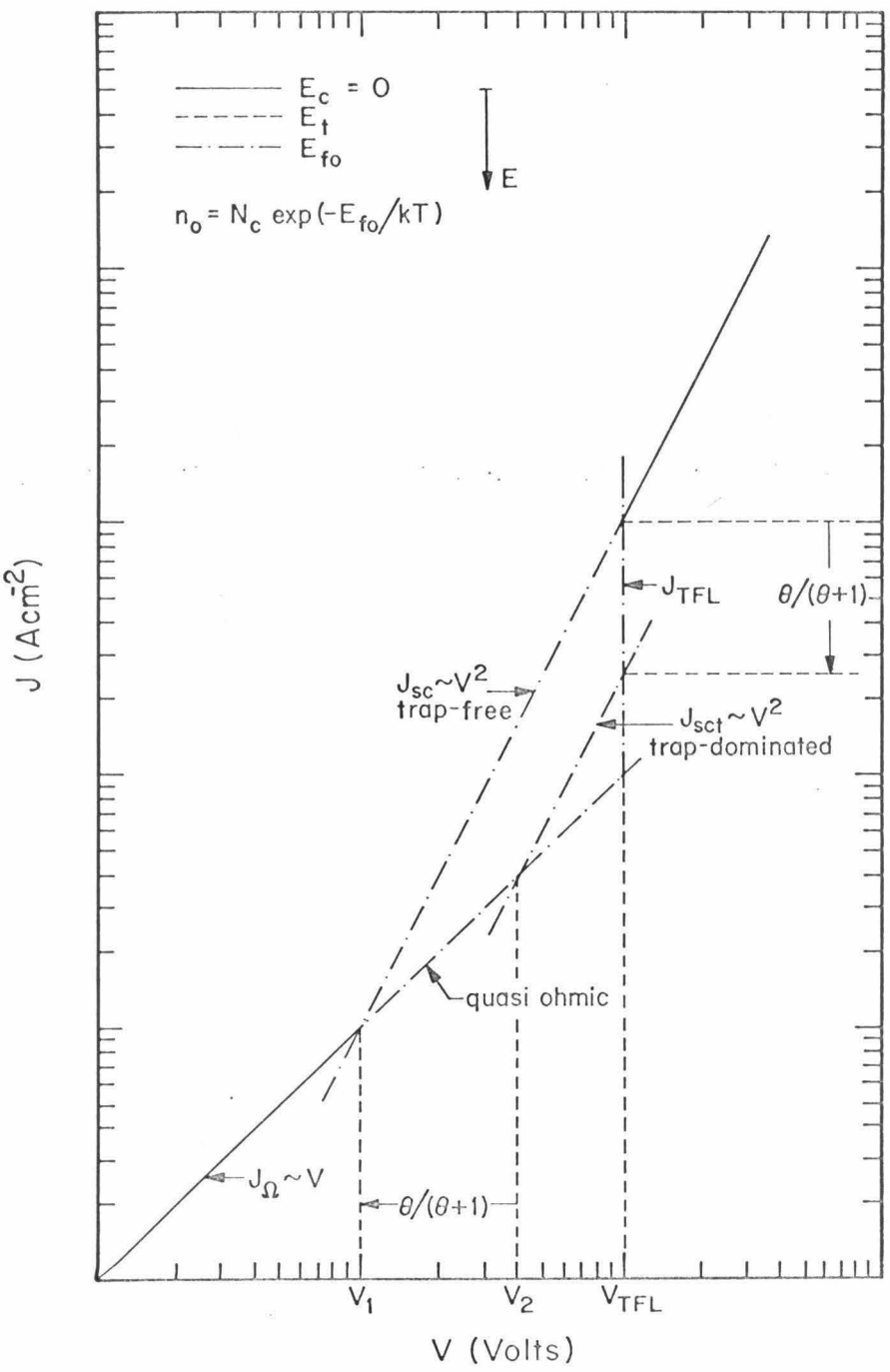

Figure 15 Idealized characteristics showing the different ranges of sclc free of traps and dominated by shallow traps.

$$n_{free} = 2n_o$$

When traps are absent, this transition occurs at the applied voltage V_1 (see Fig. 15). The corresponding position of the fermi level E_{f1} is given by

$$2n_o = N_c \exp(- E_{f1}/kT)$$

or

$$E_{f1} = E_{fo} + kT\ell n2$$

With shallow traps, however, the amount of free injected charge at V_1 is reduced by a factor of $\frac{\theta}{\theta+1}$ where θ is the statistical factor introduced in section 1.2. Hence with traps, E_{f1} is given by

$$E_{f1} = E_{fo} + kT\ell n(1+ \frac{\theta}{\theta+1})$$

For $\theta << 1$, then

$$E_{f1} \simeq E_{fo}$$

The transition between $J \sim V$ and $J \sim V^2$ in the presence of shallow traps occurs at (see Fig. 15)

$$V_2 = V_1 (\frac{\theta}{\theta+1})^{-1}$$

and the position of the fermi level E_{f2} is again given by

$$E_{f2} = E_{fo} + kT\ell n2$$

We have assumed here that the x dependence of the various carrier concentrations can be ignored. This assumption is valid some distance away from the emitter and as long as the traps are shallow, as shown by Lampert[8] and others[22]. We note in passing that, in the "quasi Ohmic" range between V_1 and V_2, the current apparently is still Ohmic but the internal conditions of the device are really those of the space-charge-limited range.

For $V_2 < V < V_{TFL}$, the concentration of the free injected charge carriers is greater than n_o. The characteristic is again "square law" until the trap-filled-limit voltage V_{TFL} is reached. In this range of applied voltage, the fermi level moves from E_{f2} to the trap level E_t. If $V_2 \simeq V_1/\theta \geq V_{TFL}$, however, the characteristic will go directly from J_Ω to J_{TFL}, and in this situation, the thermal equilibrium fermi level is only one or two kT below the trap level, i.e. the level is "deep". We recall here that a trap level is "shallow" if it is located energetically several kT above the thermal equilibrium fermi level (section 1.2).

3.3.2 Discussion of DC characteristics.

In Fig. 16 the DC characteristics of device J2 (W = 124 μ) are plotted with temperature as a parameter.

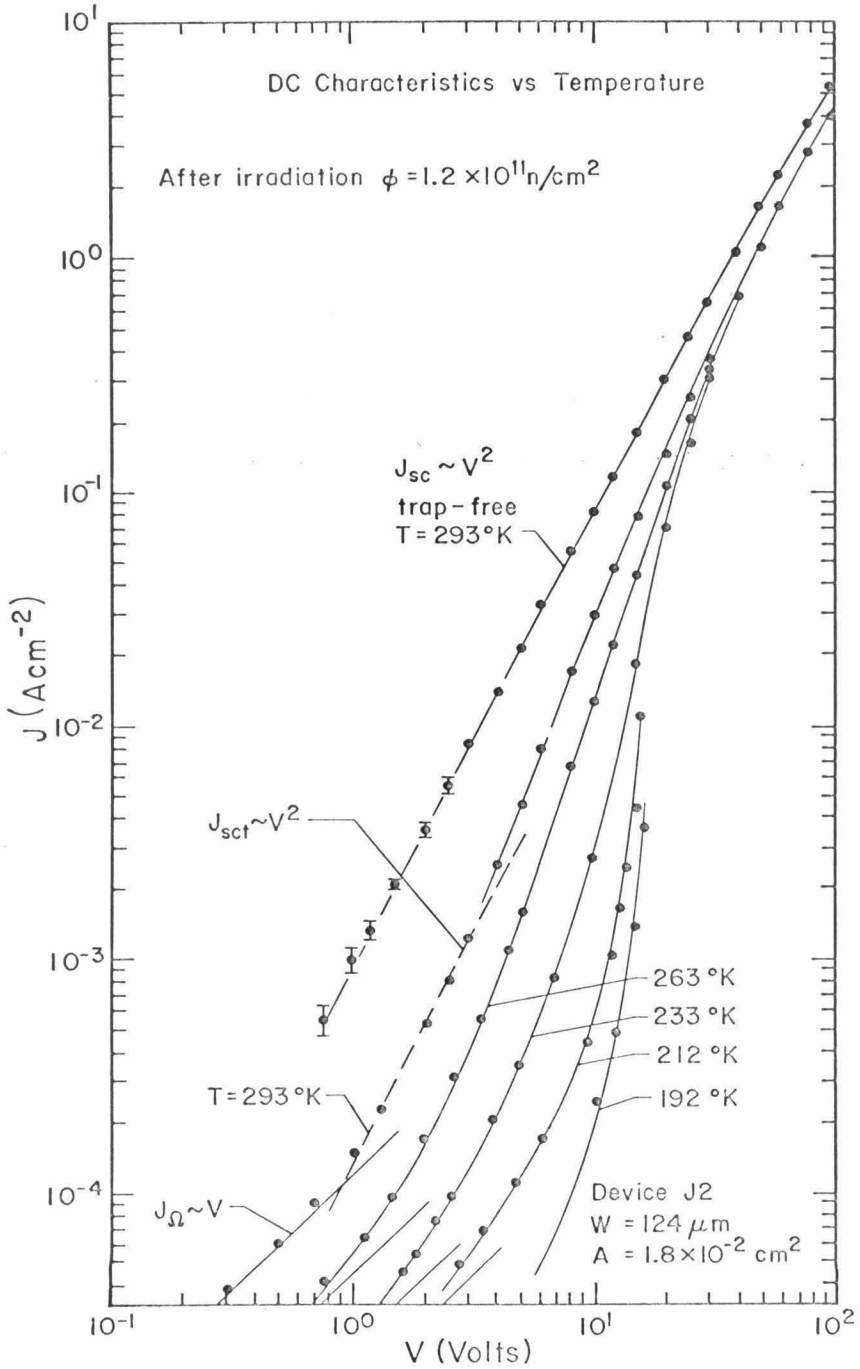

Figure 16 Typical characteristics of the DC current vs voltage as a function of temperature after irradiation at a dose of $\phi \simeq 1.2 \times 10^{11} n/cm^2$, showing the trap-filled-limit voltage.

Experimentally, we observe a square law range at T ≃ 293°K. This indicates that the traps are shallow. From the characteristics, we also obtain $V'_{TFL} \simeq 20$ V (± 10%), $\theta' \simeq 1/7$. Hence by Eq. (6) Section 1.2 we obtain the trap concentration*

$$N'_t \simeq 1.6 \times 10^{12} \text{ cm}^{-3} \qquad \text{(R-1)}$$

Thus, by Eq. (5) Section 1.2 and with $N_c = 2.4 \times 10^{19} \text{cm}^{-3}$, we calculate

$$E'_t \simeq 0.47 \pm 0.01 \text{ eV} \qquad \text{(R-2)}$$

Furthermore, from Fig. 16, we obtain

$$V_1 \ (293^{\circ}\text{K}) \simeq 0.13\text{V}$$

At T = 263°K, this same level would generate a

$$\theta' \ (263^{\circ}\text{K}) = 0.014$$

Hence

$$V_2(263^{\circ}\text{K}) \simeq 9.4\text{V}$$

---

*For convenience, we label the experimentally derived values by R-1, R-2, etc.

With $V'_{TFL} \simeq 20V$, practically independent of temperature (see Section 3.3.5), we do not expect to see a well-defined square law range in the DC characteristic anymore because of the wide transition between the Ohmic and the trap-filled-limit range. Actually J_Ω also decreases with temperature (Appendix 2) and this means that more exactly

$$V_1 \ (263^oK) \simeq 1/2 \ V_1 \ (293^oK)$$

and therefore also

$$V_2 \ (263^oK) \simeq 4.7V$$

Because J_Ω decreases with temperature at a much slower rate than θ', V_2 still increases with decreasing temperature. Hence no square law range is expected for $T < 263^oK$. This agrees with the experimental facts. We further conclude that for $T < 263^oK$, the thermal equilibrium fermi level is only one or two kT below the trap level, i.e. the level is no longer a shallow trapping level for that temperature range.

3.3.3 Theoretical discussion of proposed band models and their transient responses.

Before turning to the experimental results of the transient measurements, we shall first discuss two band models as represented in Fig. 17. Each model consists of two discrete trapping levels labelled

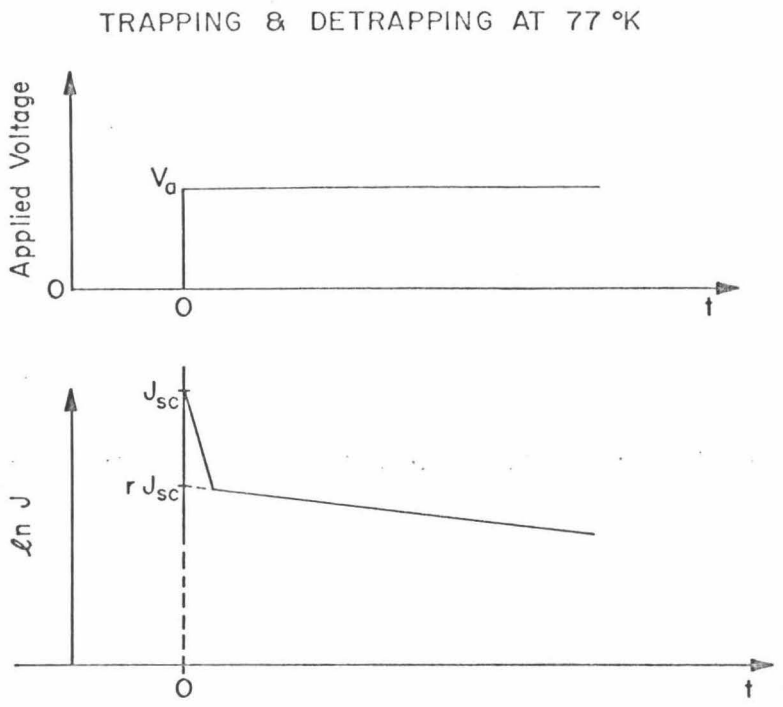

Model 1

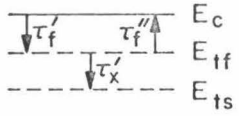

$$r \simeq \frac{\tau_f'}{\bar{\tau}}$$

$$\bar{\tau} = \frac{\tau_x' \tau_f''}{\tau_x' + \tau_f''}$$

Measured detrapping time = $\bar{\tau}$

Assumptions

$$\tau_f' \ll (\tau_f'', \tau_x')$$

$$(\tau_f'', \tau_x') \ll (\tau_s', \tau_s'', \tau_x'')$$

Model 2

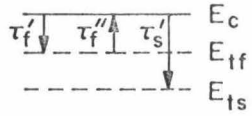

$$r \simeq \frac{\tau_f'}{\tau_f''}$$

Measured detrapping time = τ_f''

Assumptions

$$\tau_f' \ll (\tau_f'', \tau_s')$$

$$(\tau_f'', \tau_s') \ll (\tau_s'', \tau_x', \tau_x'')$$

Figure 17 Trapping models and their current response to a voltage step.

f and s with the s -level deeper than the f -level. The following nomenclature is used:

τ'_f and τ''_f for the trapping and the detrapping times of the f-level

τ'_s and τ''_s for the trapping and the detrapping times of the s-level

τ'_x and τ''_x for the downward and upward traffic time constants between the two levels.

We make the following assumptions:

Model 1: $\tau'_f << (\tau''_f, \tau'_x) << (\tau'_s, \tau''_s, \tau''_x)$

Model 2: $\tau'_f << (\tau''_f, \tau'_s) << (\tau''_s, \tau'_x, \tau''_x)$

The assumptions of model 1 imply that the trapping kinetics follows two steps. The free carriers are initially captured by the f-level, then sink into the s-level, with some fraction of the injected concentration being re-emitted into the band. The assumptions of model 2 imply that there is no traffic between the two trapping levels, but only between the levels and the conduction band. The calculations of the current response J(t) to an applied turn-on voltage step V_a, applied in the space-charge-limited range and such that $V_a << V_{TFL}$, are shown in details in Appendix 1. The results of Appendix 1 are summarized below.

In model 1, we obtain

$$J(t) \simeq J_{sc} e^{\lambda_1 t} + J_{sc} r\, e^{\lambda_2 t} \qquad (1)$$

where $J_{sc} = \frac{9}{8} \varepsilon_r \varepsilon_o \mu \frac{V^2}{W^3}$, $\lambda_1 \simeq -\frac{1}{\tau'_f}$, $\lambda_2 \simeq -\frac{1}{\tau'_x}$, $\bar{\tau} = \frac{\tau''_f \tau'_x}{\tau''_f + \tau'_x}$

and $r \simeq \frac{\tau'_f}{\bar{\tau}}$ (2)

In the detrapping experiment corresponding to this model (see discussion of experimental section 3.3.4 for details), the measured detrapping time would be $\bar{\tau}$ and the amount of carriers detrapped is $\frac{\bar{\tau}}{\tau''_f}$ N, where N is the concentration of injected carriers at the applied voltage V_a.

In model 2, we obtain

$$J(t) \simeq J_{sc} e^{\lambda_1 t} + J_{sc} r\, e^{\lambda_2 t} \qquad (3)$$

where

$$\lambda_1 \simeq -\frac{1}{\tau'_f}\,,\ \lambda_2 \simeq -\frac{1}{\tau'_s} \text{ and } r \simeq \frac{\tau'_f}{\tau''_f} = \theta_f$$

In the detrapping experiment corresponding to this model, the measured detrapping time would be τ''_f and we expect all injected carriers to be detrapped.

Experimentally, the difference in the two models appears in the results of the detrapping experiments. We will show below that, from the results of the detrapping experiments, model 1 applies to our case. These results will yield $\frac{\bar{\tau}}{\tau''_f}$ and $\bar{\tau}$. From the J(t) curves, the factor r and the trapping time τ'_f are measured. These numbers should satisfy the relation $r = \frac{\tau'_f}{\bar{\tau}}$ which serves as an internal self-consistency check. Also τ''_f can be derived, hence we can obtain

$$\theta_f = \frac{\tau'_f}{\tau''_f}$$

Once N_{tf} is known, E_{tf} and σ_f can be obtained (sections 1.2 and 1.3). We note here that if the concentration of f-level is finite, a V_{TFLf} will be reached in the plot of $(J_{sc}r)$ vs voltage which is indeed observed (Fig. 20). We also note that since τ''_f is a function of temperature, r is also a function of temperature. This last point will be used later to show that, in the high temperature range, the non-exponential behavior of the current vs time observed is not due to a distribution in energy of trap levels.

3.3.4 Discussion of experimental transient measurements.

In terms of the two-level model proposed in the preceding section, the values of N'_t and E'_t (R-1 and R-2) are associated with the s-level and will be used as N_{ts} and E_{ts}. As will be shown later, this s-level has a slow average trapping time at 77^oK compared to a fast trapping time associated with the f-level at the same temperature.

Fig. 18 shows the current response $J(t)-J(\infty)$ to a turn-on voltage step of $V_a = 5$ V for device J2. Temperature is the parameter. The increase in current at $t \simeq 0$ as a function of temperature reflects the temperature dependence of the mobility, as discussed in section 3.2.1. In Fig. 19, this effect is eliminated by normalizing the curves to the room temperature mobility.

At $T = 293^oK$, the time dependence of the current is fairly closely exponential. Since θ_s is small, we derive (Eq. 7 section 1.3)

$$\tau'_s \simeq 4.3\ \mu s$$

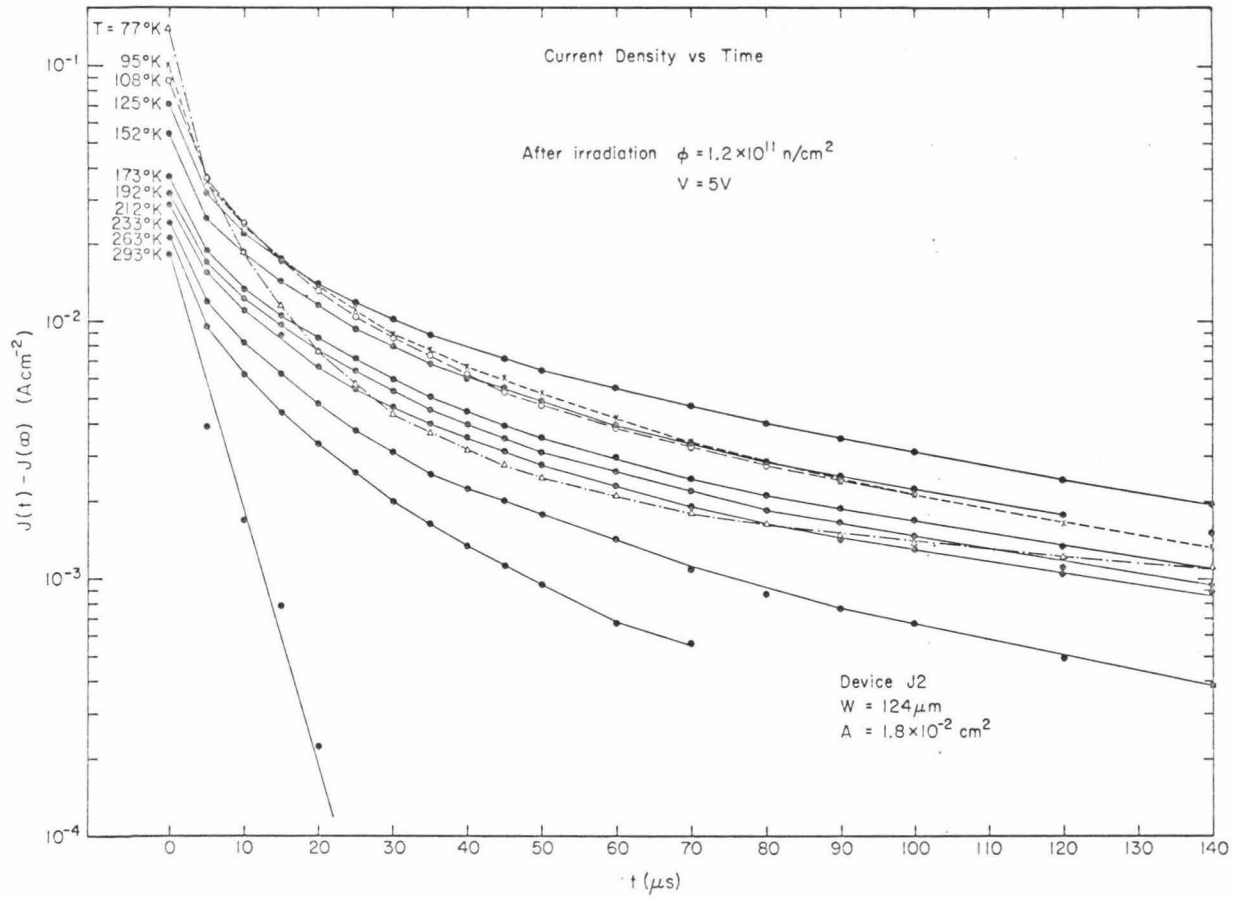

Figure 18 The dependence upon time of the current J(t)-J(∞) for a constant voltage step of 5V applied at t ≃ 0 to a thick device having V_{TFL} ≃ 20 V. Temperature is the parameter.

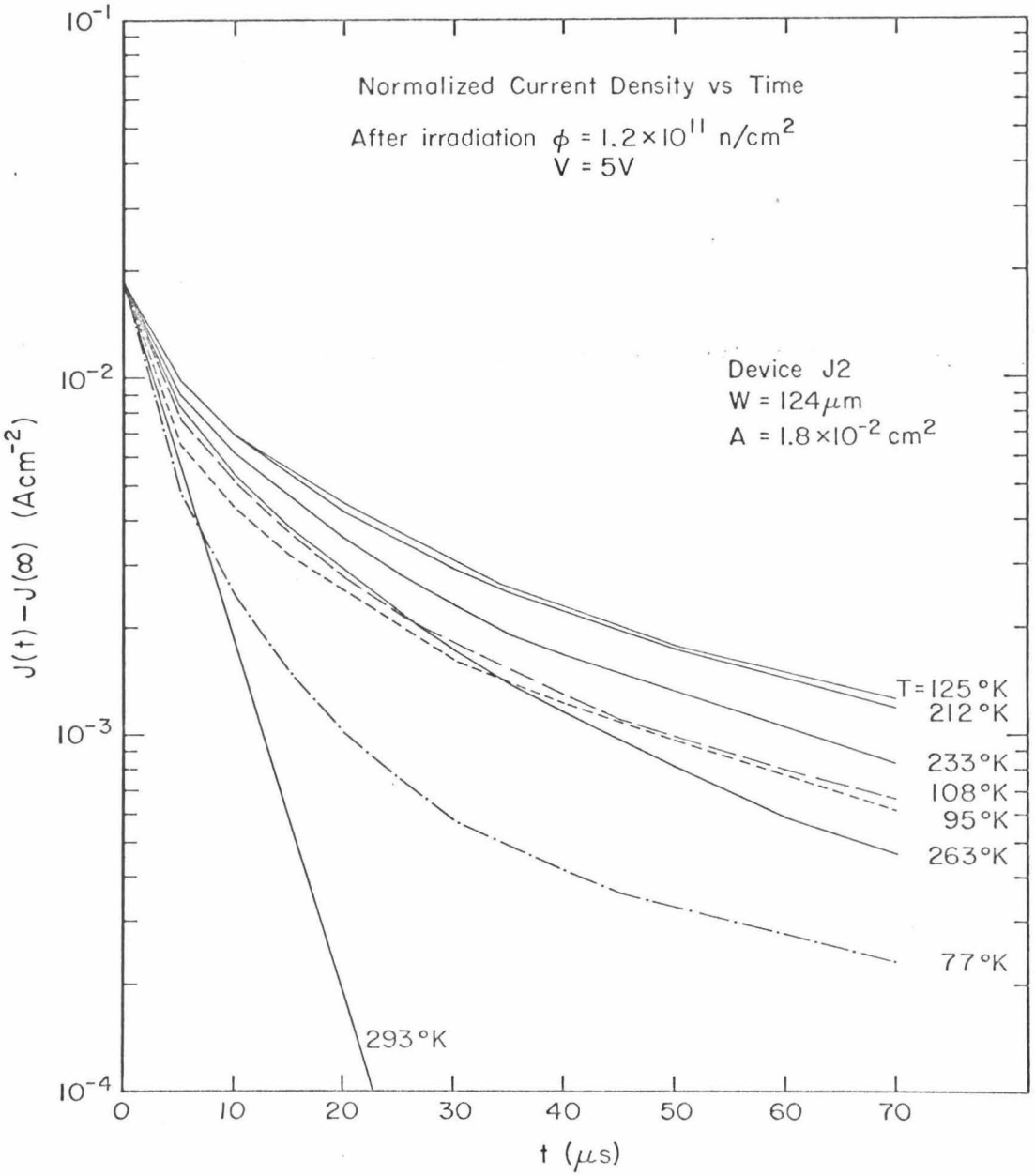

Figure 19 The dependence upon time of the current J(t)-J(∞) normalized to the room temperature mobility, for a constant voltage step of 5V applied at t = 0 to a thick device having $V_{TFL} \simeq 20$ V. Temperature is the parameter.

Hence with $N_{ts} \simeq 1.6 \times 10^{12} cm^{-3}$ and $V_{th} = 10^{7} cm/s$ the capture cross-section of the 0.47 eV level at $T = 293^{o}K$ (Eq. 8 section 1.3) is

$$\sigma_s \simeq 1.45 \times 10^{-14} \ cm^2 \qquad (R-3)$$

This order of magnitude indicates that the trap is an attractive coulombic center. In fact, the capture cross-section of an attractive Coulomb center can be estimated from the following relation[23]

$$\sigma = \frac{2\pi}{\ell} \left(\frac{q^2}{8\pi\varepsilon kT}\right)^3$$

where $\ell = 7.1 \times 10^{-9} \mu$, in unit of cm, is the mean free path in the thermal agitation range, ε is the dielectric constant of silicon and σ is in unit of cm^2. With $\mu = 1.35 \times 10^{3} cm^2/Vs$ at room temperature, we obtain

$$\sigma \simeq 1.4 \times 10^{-14} \ cm^2$$

Thus it is very likely that the trapping state observed at 0.47 eV is singly positively charged when not occupied by a trapped electron.

In the temperature range $125^{o}K < T < 263^{o}K$, the J(t) curves are non-exponential and hardly change with temperature. It is not likely that this non-exponential behavior is due to a distribution of levels since this interpretation would require a change in J(t) with temperature (see section 3.3.3). It is not due to the saturation of traps

either, because according to Gregory et al[11] the decay is closely exponential when $V \simeq (1/4)\ V_{TFL}$. We have, however, already noted that in this temperature range, the 0.47 eV level is no longer shallow. In that instance the occupancy of the level varies appreciably with x, even at thermal equilibrium and certainly more so during the transient. A theory for the transient response under such circumstances does not yet exist, but it is to be expected that the decay will not follow a simple exponential anymore in this case.

We note that, as temperature decreases, other trapping levels shallower than the 0.47 eV level could start to influence the current. This happens when their associated factor θ (Eq. 5 section 1.2) becomes smaller than 1. Indeed, in the temperature range $77^{o}K < T < 110^{o}K$, the J(t) curves have an additional fast component indicating the presence of another level according to our models (Appendix 1). The results of Appendix 1, as summarized in Section 3.3.3, are strictly correct only for shallow traps. In applying them to our case where one of the levels is deep, the procedure is thus one of mere first approximation. A typical form of the fast component at $77^{o}K$ is plotted in Fig. 20. The fast time constant lies at about 3μs. The non-exponential behavior of this fast decay is probably related to the non-ideal situation which exists in reality. Fig. 21 shows the value of J_{scf} (i.e. J_{scr} of theoretical discussion) of the current after the fast decay only and the current at DC ($J_{sc\ total}$) at $77^{o}K$. A trap-filled-limit voltage is observed for J_{scf}. Although V_{TFLf} is defined only approximately by the characteristic J_{scf} (V), the values of V_{TFLf}

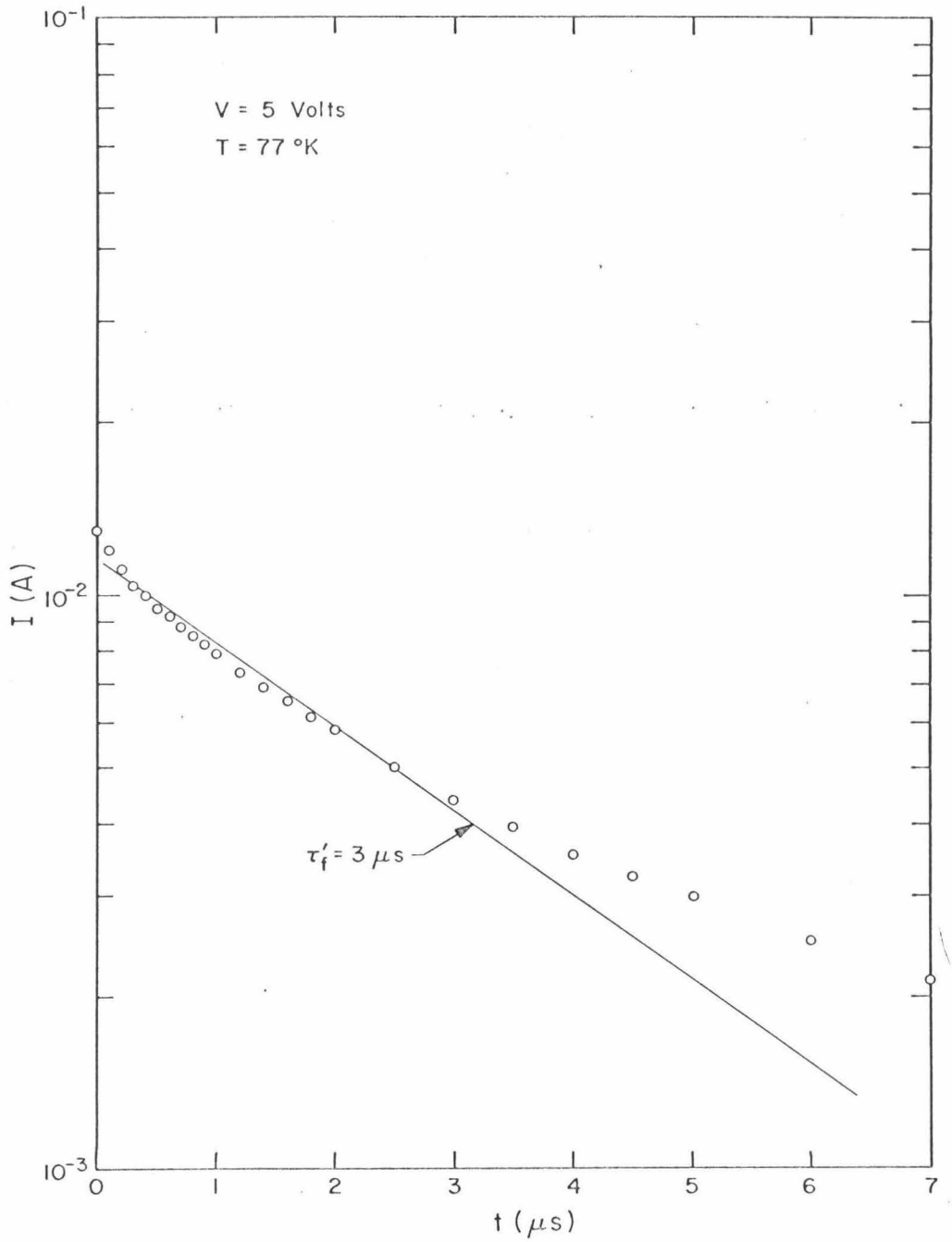

Figure 20 The initial portion of current vs time at 77°K, after irradiation at a dose of $\phi \simeq 1.2 \times 10^{11} n/cm^2$, as a response to a voltage step 5V. V_{TFL} of this device is at about 20V.

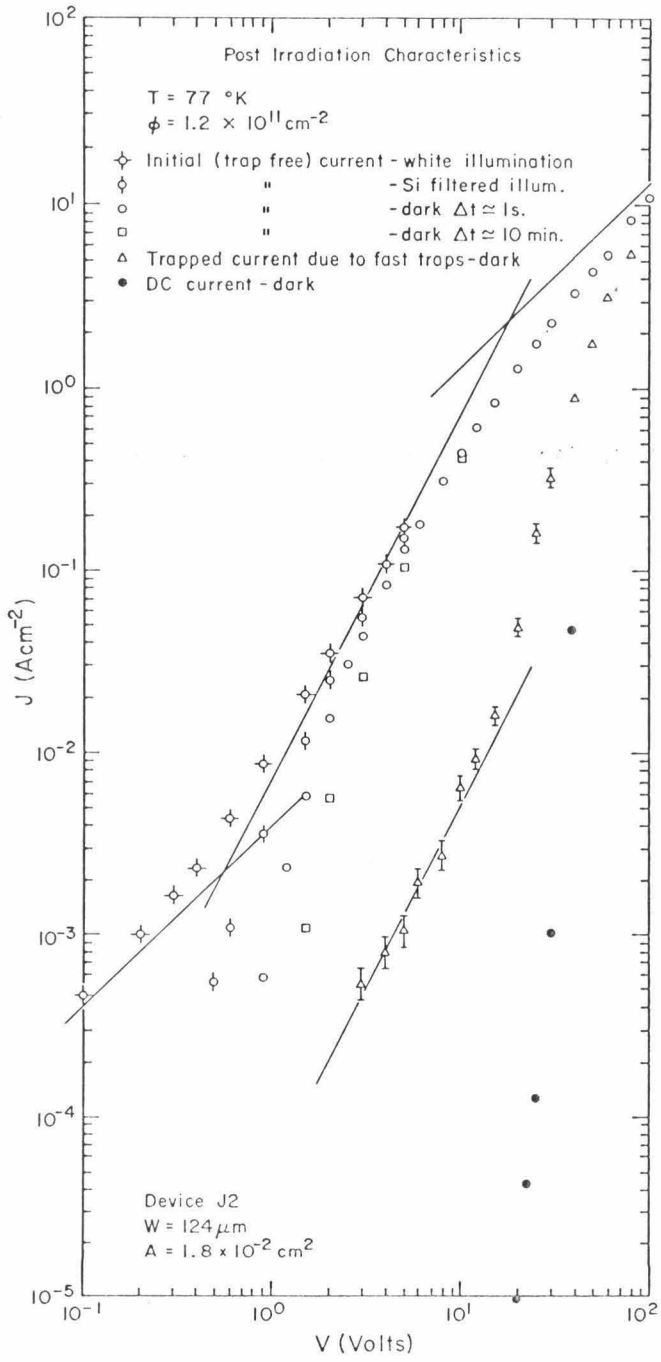

Figure 21 Typical characteristics of initial (trap-free) current vs voltage at 77°K, after irradiation at a dose of $\phi \simeq 1.2 \times 10^{11} n/cm^2$, obtained under various conditions of ambient illuminations. Also shown are the characteristics of J_{scf} (open triangles) and of $J_{sc\ total}$ (full dots). The steep rises in current indicate the position of V_{TFLf} and $V_{TFL\ total}$, respectively.

of various devices show a clear W^2 dependence on the thickness (Fig. 22). This offers support to the two level idea. Analogous results holds for $J_{sc\ total}$ and $V_{TFL\ total}$.

The concentration of the f-level follows directly from V_{TFLf} and we obtain (Eq. 6 Section 1.2)

$$N_{tf} \simeq 1.4 \times 10^{12} cm^{-3} \qquad \text{(R-4)}$$

With a trapping time τ'_f around 3μs and with this concentration N_{tf}, we derive a capture cross-section of (Eq. 8 Section 1.3)

$$\sigma_f \simeq 4 \times 10^{-14} cm^2 \qquad \text{(R-5)}$$

using the value of $v_{th} = 0.6 \times 10^7$ cm/s for the thermal velocity at 77^oK. This magnitude for σ_f again indicates an attractive coulombic center.

To check our models (Fig. 17), the following detrapping experiment is performed at 77^oK. A turn-on voltage step V_a is applied. The voltage is then suddenly reduced to zero before J(t) has reached the end of the fast decay. Let the current density at this instant of time be J_{off} (as shown in Fig. 23). According to both models in Fig. 17, the injected charge is now mostly trapped in the f-level which is faster than the s-level. Within a transit time of the instant t = 0 when the device is short-circuited, all carriers in the conduction band are

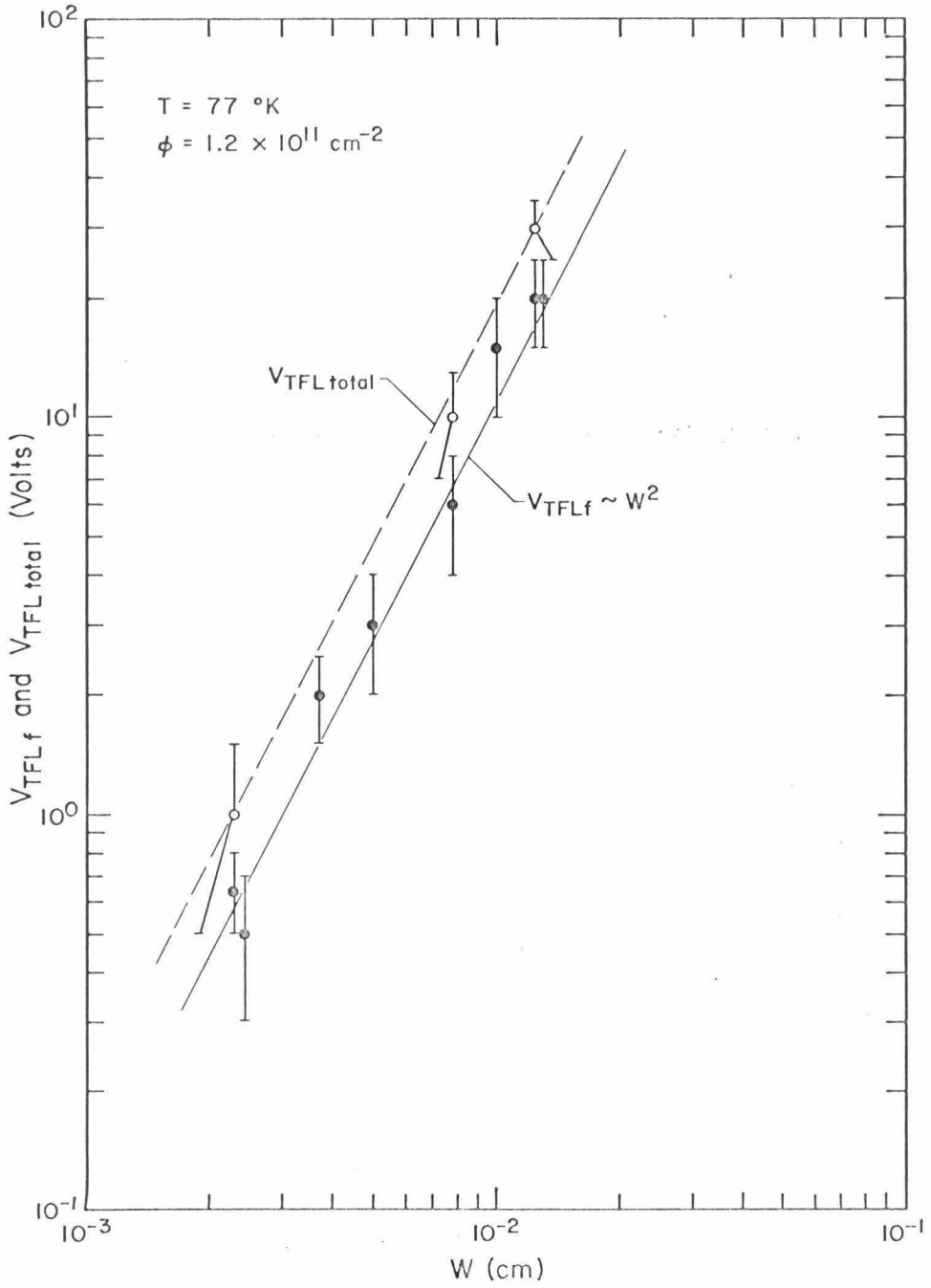

Figure 22 The dependence upon the thickness W of V_{TFLf} and $V_{TFL\ total}$.

Current Response in the Double Pulse Experiment

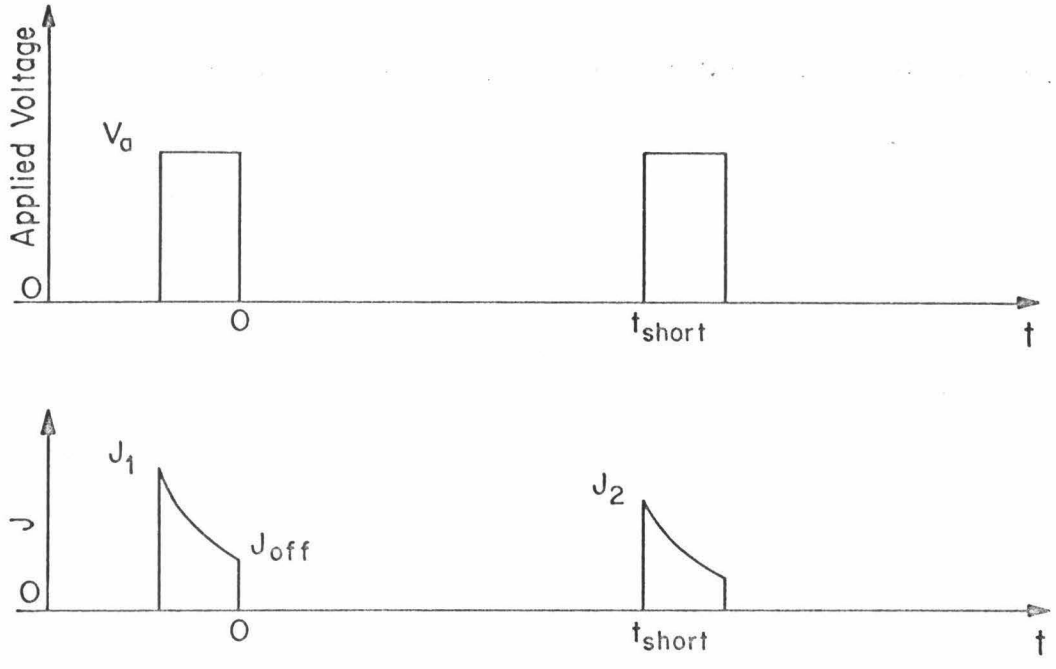

Figure 23 Diagram of the current responses to the voltage pulses applied in the detrapping experiments.

swept out by the internal electric field generated by the trapped charge. As time goes on, carriers are detrapped thermally and are swept out by the field of the remaining trapped charge. Hence, as carriers are detrapped the transit time in the field of the trapped charge increases rapidly. It is shown in Appendix 1, however, that this whole process is much shorter than the time periods considered here. We can thus assume that all carriers in the conduction band are swept out of the device before they could be retrapped during the time the device is short-circuited.

If now at $t = t_{short}$, a second pulse V_a is applied, the difference between the maximum amplitude J_2 of the second current pulse and J_{off} is directly proportional to the concentration of carriers detrapped in the time interval $0 < t < t_{short}$ (Fig. 23). That it is so is shown by the following argument.

With an applied voltage V_a, the total injected charge Q_1 is approximately given by

$$Q_1 \simeq CV_a$$

where C is the geometrical capacitance per unit area of the device. The current J_1 is given by

$$J_1 \simeq Q_1/t_o$$

where t_o is the transit time

$$t_o = W^2/\mu V_a$$

Let us assume that at $t = 0$ (when the device is short-circuited) Q_1 is completely trapped. Suppose that fQ_1 is detrapped during the time interval $0 < t < t_{short}$. When a second voltage pulse V_a is applied at $t = t_{short}$, the total charge in the device must again be Q_1. Since fQ_1 had escaped, that amount is added by injection of free carriers at $t = t_{short}$. Hence the current J_2 will be

$$J_2 = fQ_1/t_o = fJ_1$$

Hence we have shown that the amplitude of the current of the second pulse is directly proportional to the amount of detrapped carriers. Therefore it is only necessary to analyze the height of the second current pulse in order to find out about the amount of carriers detrapped in the time interval $0 < t < t_{short}$.

Experimentally we observe that the height of the second current pulse J_2 increases roughly exponentially with t_{short}. The average time constant is about 300μs and reaches the limiting value

$$J_2\ (t_{short} = \infty) \simeq 1/4\ (J_1 - J_{off}) + J_{off}$$

The average detrapping time constant is chosen as the time it takes J_2 to reach the value $\{J_{off} + 0.63\ [J_2(t_{short} = \infty) - J_{off}]\}$.
This result indicates that only 1/4 of the trapped injected charge is detrapped. Hence, model 1 applies, since model 2 predicts that the majority of the trapped charge in this experiment should detrap (Appendix 1). Therefore we have from model 1

$$\frac{\bar{\tau}}{\tau''_f} = \frac{1}{4} \qquad \text{(R-6)}$$

The measured detrapping time constant is

$$\bar{\tau} \simeq 300 \pm 50\ \mu s \qquad \text{(R-7)}$$

and the factor r is measured to be (Fig. 21)

$$r \simeq 0.01 \qquad \text{(R-8)}$$

We have found $\tau'_f = 3\mu s$. This allows us to make an internal self-consistency check of the value of r (R-8) using the values of τ'_f and $\bar{\tau}$ (R-7). The relation $r = \frac{\tau'_f}{\bar{\tau}}$ is indeed satisfied. Using the experimental values above, we derive

$$\tau'_x \simeq 400\ \mu s$$

$$\tau''_f \simeq 1200 \mu s$$

hence

$$\theta_f \simeq \frac{1}{400} \qquad \text{(R-9)}$$

With $N_{tf} \simeq 1.4 \times 10^{12} cm^{-3}$, E_{tf} is derived to be (Eq. 5 Section 1.2)

$$E_{tf} \simeq 0.14 \text{ eV} \pm 0.005 \text{ eV} \qquad \text{(R-10)}$$

Another internal consistency check is applied as follows.

The temperature T_o at which this 0.14 eV level will start to act visibly as a trap, i.e. when the corresponding factor $\frac{\theta_f}{\theta_f+1} < 1$, can be estimated. We have (Eq. 5 Section 1.2)

$$T_o = E_{tf}/(k\ell n \frac{\theta_f N_{tf}}{N_c})$$

With $E_{tf} \simeq 0.14$ eV, $N_{tf} \simeq 1.4 \times 10^{12} cm^{-3}$, $N_c \simeq 3 \times 10^{18} cm^{-3}$ and setting $\theta_f = 1$, we derive

$$T_o \simeq 108^{o}K$$

This is indeed closely the temperature at which additional trapping is observed in Fig. 18 and 19, and thus constitutes an independent confirmation of the proposed two-level model. Thus, there exists two regimes of trapping behavior. In the temperature range $108^{o}K < T < 293^{o}K$, only the s-level (0.47 eV) influences the current, while in the temperature

range $77^{o}K < T < 108^{o}K$, both f-level (0.14 eV) and s-level influence the current. Some further experimental data consistent with the two-level model are given below.

In the temperature range $200^{o}K < T < 293^{o}K$, the following detrapping experiment is performed: a long voltage pulse ($\sim$ 250μs) is applied and is immediately followed by a short-circuit condition. At time $t = t_{short}$ from the end of the first pulse, a second voltage pulse is applied. The amplitude J_2 of the second current pulse is again directly related to the amount of charge detrapped in the time interval $0 < t < t_{short}$. We observe that J_2 increases roughly exponentially with t_{short} and, in the limit of $t_{short} \to \infty$, reaches a limiting value equal to J_1, i.e. all the charge is detrapped. In this temperature range, the only detrapping time constant involved is τ''_s since, according to our model, the fast 0.14 eV level is too shallow to alter the process significantly. The measured detrapping time constant (measured in the same way as in the detrapping experiment at $77^{o}K$) as a function of temperature is listed in table III. The calculated detrapping time constant (Appendix 1) as a function of temperature is also listed, taking for τ'_s the experimentally determined values (Fig. 16) and using $E_{ts} = 0.475$ eV. The agreement between $\tau''_{s\ meas}$ and $\tau''_{s\ calc}$ is good, and hence this result is consistent with the proposed model. Besides, it confirms the value of the energy depth of the s-level.

TABLE III

Trapping and Detrapping Time Constants in the High Temperature Range

T	$293^{o}K$	$263^{o}K$	$233^{o}K$	$212^{o}K$
τ'_{meas} (μs)	4.3	15	30	30
τ''_{meas} (μs)	23	100	500	7400
τ''_{calc} (μs)	28	95.5	720	7100

3.3.5 Analysis of additional data.

At $77^{o}K$ we had measured $J_{sc\ total}$ and obtained $V_{TFL\ total}$ which is the trap-filled-limit voltage corresponding to the total concentration of traps $N_{t\ total} = N_{tf} + N_{ts}$ at $77^{o}K$.

From $V_{TFL\ total}$ we obtain

$$N_{t\ total} \simeq 2.4 \times 10^{12} cm^{-3}$$

to within 10%. Hence the concentration of 0.47 traps at $77^{o}K$ is

$$N_{ts} = N_{t,\ total} - N_{tf}$$

$$\simeq 1 \times 10^{12} cm^{-3}$$

to within 20%. All these values are from $77^{o}K$ data. At room temperature, however, we found for the concentration of the same s-level

$$N_{ts} \simeq 1.6 \times 10^{12} cm^{-3}$$

to within 10%. This change must thus reflect a fermi level shift as a function of temperature. It means that at $77^{o}K$, about 1/3 of the 0.47 eV traps are occupied at thermal equilibrium, assuming that at room temperature this occupancy is negligible. This large occupancy

of the 0.47 eV levels at 77°K at thermal equilibrium is consistent with earlier facts. At the beginning of this section, we had indeed found that, at low temperatures, the thermal equilibrium fermi level is very close to the 0.47 eV level (this level is "deep" at low temperatures), thus leading to appreciable occupancy.

In Fig. 24, N_{tf} is plotted as a function of irradiation dose ϕ. The data point at $\phi \simeq 1.2 \times 10^{11} n/cm^2$ is the result of the analysis of 8 samples. The data points at $\phi \simeq 5.5 \times 10^{11} n/cm^2$ and $\phi \simeq 4 \times 10^{12} n/cm^2$ are obtained from the analysis of 2 samples. From Fig. 24, we derive an introduction rate of $\sim 11\ (ncm)^{-1}$ for the 0.14 eV level. The introduction rate measured at 77°K for the 0.47 eV level is $\sim 8\ (ncm)^{-1}$, obtained from the analysis of 8 samples at $\phi \simeq 1.2 \times 10^{11} n/cm^2$, 2 samples at $\phi \simeq 5.5 \times 10^{11} n/cm^2$ and none at $\phi \simeq 4 \times 10^{12} n/cm^2$, the reason being that at $\phi \simeq 4 \times 10^{12} n/cm^2$, $V_{TFL\ total}$ exceeds the breakdown voltage of the sample.

Preliminary annealing experiments indicate that even after anneal at 350°C, strong trapping by the 0.47 eV level still occurs. This point will be discussed further in the next section.

3.3.6 Summary and discussion.

In the preceding section, we have studied the trapping and the detrapping processes which exist in silicon single crystals after irradiation with fast neutrons. We have identified two distinct trapping levels at about $E_{tf} \simeq 0.14$ eV and $E_{ts} \simeq 0.47$ eV below the conduction band. They are introduced at rates of $\sim 11\ (ncm)^{-1}$ and

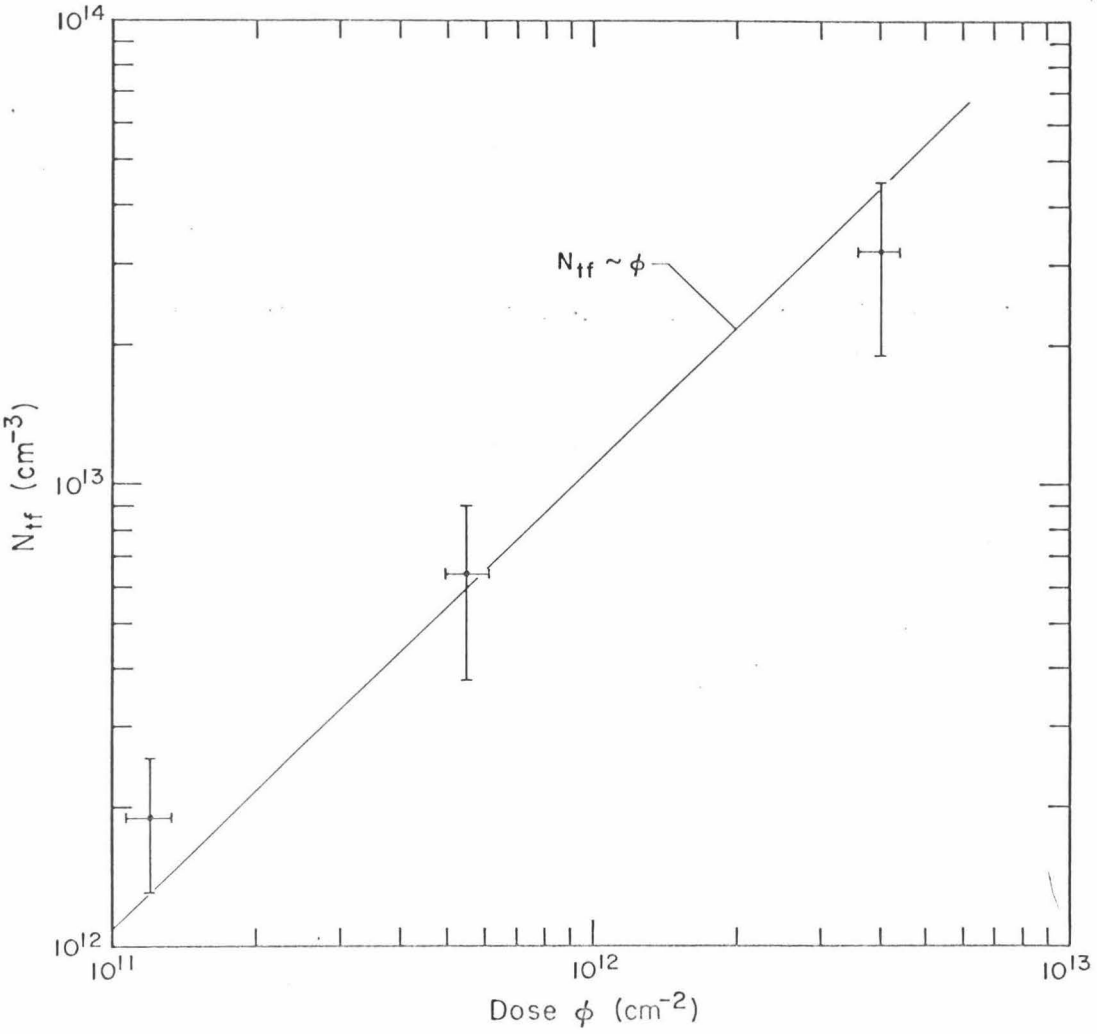

Figure 24 The dependence upon dose of the concentration of fast traps at 77°K. The straight line indicates an introduction rate of ∿11 (ncm)$^{-1}$.

$\sim 8\ (ncm)^{-1}$ respectively, yielding concentrations of $\sim 10^{12} cm^{-3}$ for a dose of $\phi = 1.2 \times 10^{11} n/cm^2$. The cross-sections of $\sigma_f = 4 \times 10^{-14} cm^2$ at $77^{\circ}K$ and $\sigma_s \simeq 1.4 \times 10^{-14} cm^2$ at room temperature indicate that both levels are of the donor type (that is, singly positively charged when empty). Since the free carrier concentration after irradiation, (Appendix 2) computed from the Ohmic current, does not exceed $\sim 10^{11} cm^{-3}$, we conclude that, from neutrality requirement, there must also exist acceptor type levels introduced by the radiation. At $77^{\circ}K$, the trapping kinetics follows two steps. The free electrons are initially captured by the shallow 0.14 eV traps and then sink into the deep 0.47 eV traps, predominantly without being re-emitted into the band. Above approximately $110^{\circ}K$, the shallow traps are not numerous enough and their detrapping rate is sufficiently fast so that the deep traps dominate the transient response. Table IV summarizes the findings. The proposed model describes the majority of experimental observations satisfactorily and self-consistently. It explains, for example, why we observe a characteristic composed of an Ohmic range followed by a square law range then by a trap-filled-limit range, at room temperature, and a characteristic composed of an Ohmic range followed immediately by a trap-filled-limit range, at low temperatures. It also properly represents detrapping characteristics both as a function of time and temperature.

The experimental results presented here also offered a first direct verification of the simple model of space-charge-limited current

TABLE IV

Summary of Results of Trapping Phenomena in Silicon

Due to 14 MeV Neutron Radiation

	"fast" traps	"slow" traps
Energy below conduction band	$E_{tf} = 0.14 \pm 0.005$eV	$E_{ts} = 0.47 \pm 0.01$eV
Introduction rate at 77°K	$\sim 11\ (\text{ncm})^{-1}$	$\sim 8\ (\text{ncm})^{-1}$
Concentration	$N_{tf} \simeq 1.4 \times 10^{12}\text{cm}^{-3}$ at 77°K	$N_{ts} \simeq \begin{matrix} 1.0 \times 10^{12}\text{cm}^{-3} \text{ at } 77^{\circ}\text{K} \\ 1.6 \times 10^{12}\text{cm}^{-3} \text{ at } 293^{\circ}\text{K} \end{matrix}$
Capture cross-section	$\sigma_f \simeq 4 \times 10^{-14}\text{cm}^2$ at 77°C	$\sigma_s \simeq 1.4 \times 10^{-14}\text{cm}^2$ at 293°K
Trapping time constants	$\tau'_f \simeq 3\mu$s at 77°K	$\tau'_s \simeq 4.3\mu$s at 293°K
Detrapping time constants	$\tau''_f \simeq 1200\mu$s at 77°K	$\tau''_s \simeq 23\mu$s at 293°K

dominated by shallow and deep traps. There exists no case in the open literature in which the characteristic of space-charge-limited current through a solid has successfully been interpreted with a finite number of discrete trapping levels. In the few cases in which both a trap-free ($V >> V_{TFL}$) and a trap-dominated ($V << V_{TFL}$) range have actually been observed, the transition was so broad that a continuous distribution of traps throughout a band of energies had to be invoked for an explanation[24]. Although we do not claim that bands do not really exist in the present case, the analysis offered in this chapter indicates that if they exist, these bands are fairly narrow and sufficiently so, that a discrete level offers an acceptable approximation to reality.

Several experimental facts have not found a simple explanation, however: (i) the predominantly non-exponential nature of the time dependences for temperatures below 263^{o}K, (ii) the threshold voltage observed in the initial current characteristics in the same temperature range, and (iii) the temperature dependence of the current in the Ohmic range (Appendix 2). We think that the first two are related because they start to occur in the same temperature range. Attempts to explain the non-exponential behavior as due to many traps distributed in energy soon develop inconsistencies. We have pointed out in section 3.3.2 the correlation between the non-exponential time dependence and the fact that the 0.47 eV level is only one or two kT above the thermal equilibrium fermi level. When this situation prevails, one can certainly no longer neglect the spatial dependence of the trap population. No theory exists for the large signal turn-on transient response under

these conditions. Clearly, the problem is no longer linear, and exponential solutions cannot be expected. An approach to this problem which could avoid elaborate analyses, as computation would, consists of subdividing the bulk into "uniform" segments, blur the discontinuities and thus finally end up with sums of exponentials. This analysis has not been performed. It is clear that the next major improvement on this study would consist in studying this non-exponential behavior. This might involve a detailed analysis of the influence of defect clusters in silicon[25].

The experimental techniques conventionally used to analyze irradiated silicon are the Hall Effect and resistivity measurements as a function of ambient temperature. These methods all test thermal equilibrium conditions. In this study, the Ohmic range corresponds to a thermal equilibrium situation. However, the Ohmic characteristics are not understood at present (Appendix 2). On the other hand, our space-charge-limited current technique, definitely does not qualify for this statement. Whether space-charge-limited current can be regarded as an extension of thermal equilibrium, and under what conditions, is a matter presently under discussion in connection with noise measurements of space-charge-limited current. It would be very valuable, in the context of this work, to possess guidelines and means with which to establish quantitative connections between space-charge-limited current and thermal equilibrium measurements. The problem may, unfortunately, be rather complex. For instance, recombination and generation phenomena will necessarily have to be included also. But theories of

single carrier space-charge-limited current which would incorporate the effect have not yet been developed. Theories of double injection (two-carrier space-charge-limited current), on the other hand, typically assume that recombination is the main rather than a secondary effect.

Fast neutron damage in silicon has been studied previously by other workers[26 - 31]. In contrast to ours, their results are always obtained on silicon of much lower resistivity and generally under conditions near thermal equilibrium. There are two types of defects to be considered: intrinsic defects or defects related to the silicon itself, and impurity related defects or defects that are associated with the chemical impurities present in the lattice. A common defect in phosphorous-doped silicon is the vacancy--phosphorous complex which has a level at 0.47 eV. Preliminary results of annealing experiment performed on our devices indicate that at least a fraction of the traps identified at 0.47 eV is attributable to the vacancy-phosphorous complex; however, the remainder seems to be related to intrinsic defects because even after annealing at temperatures much higher than the annealing stage for the vacancy-phosphorous complex (the V-P complex anneals at around 120^{o}C), trapping by the 0.47 eV level is still observed. To our knowledge, the 0.14 eV level has not been identified before in fast neutron-damaged silicon. It probably is also related to intrinsic defects rather than impurity related defects.

Finally, the results have direct practical significance. It can be stated that devices exposed to fast neutron radiation will not be affected seriously in their performance as far as changes in the mobility is concerned. But the trapping of carriers will quite soon have serious detrimental effects if the devices operate with space-charge-limited current. It thus does not follow that, if a device relies only on the drift of one type of carriers (rather than on the presence of two, as in a conventional transistor), that device will also be radiation resistant. This point has been generally overlooked so far, but is obviously quite significant.

CONCLUSION

The flow of space-charge-limited current through high purity silicon has been analyzed before and after the introduction of defects by 14 MeV neutron radiation. The effect of the radiation on the drift velocity-field relationship of electrons in silicon is studied. The number of data points is, however, too limited to allow a detailed analysis of this effect and no formal description of it is given. The presence of trapping levels introduced by the radiation is established with transient and DC measurements of space-charge-limited current. These measurements yield information on their trapping kinetics. Double pulse detrapping experiments are performed to study their detrapping characteristics. A band model consisting of two discrete trapping levels is proposed. This model explains self-consistently the majority of the experimental data very well.

The results presented here have implications in device application of space-charge-limited current. They establish that devices operating on sclc are sensitive to radiation mainly due to the introduction of traps. These results also attest to the sensitivity of sclc as a tool to study radiation effects in solids. Sclc is a non-thermal equilibrium method of analysis. At this time, it is not clear how our sclc data are related to data obtained with more conventional thermal equilibrium measurements like Hall effect and resistivity measurements.

The choice of neutron in this work was one of mere convenience. The cluster nature of fast neutron damage could be the cause of some of the unanswered problems raised in this work. It would be interesting to study the flow of sclc through γ-irradiated silicon, for instance, since γ rays are known to introduce more elemental defects rather than damage clusters.

The unanswered problems raised in this work are several. The problem of current transient response of sclc in the presence of deep traps is one. This problem, in general, might not be solvable analytically due to its non-linear nature. The temperature dependence of the Ohmic current in our devices is another problem which remains to be understood. These several new directions for future work again attest to the usefulness of sclc as a tool to study radiation damage in solids.

APPENDIX I

Trapping and Detrapping Models

As Lampert has shown[8], as long as the fermi level is several kT below the trap levels, space-charge-limited current J_{sc} is given at steady state by

$$J_{sc} = J_{anode} \simeq n_a e\mu E_a$$

where the subscript "a" refers to quantities measured at the anode. Hence for a constant applied voltage V_a resulting in a constant E_a, J_{sc} is about proportional to n_a. In other words, the x dependence can be ignored. This conclusion by Lampert is verified by numerical computations done by Wright and others[22]. Furthermore, Many and Rakavy[9] have shown that in the case of slow trapping i.e. when trapping is slow compared to the transit time, the transient problem for times longer than the transit time reduces to that of a sequence of steady state conditions. Therefore the problem of current vs time can be reduced to the problem of free carrier concentration vs time independently of x as long as (i) the trap levels are shallow, that is the trapping time constants do not significantly vary with x and (ii) the time scale is always long compared to the transit time of a free carrier (slow trapping assumption).

In this appendix we analyze two models of trapping and detrapping with the above assumptions. τ' and τ'' are the trapping and detrapping time constants respectively. The subscripts f, s and x serve to differentiate between different levels (see Fig. 17).

Consider the trapping process in model 1. The three important time constants are τ'_f, τ''_s, τ'_x. All other trapping and detrapping time constants are assumed to be much larger than any of these. The differential equations are

$$\frac{dn}{dt} = -\frac{n}{\tau'_f} + \frac{n_f}{\tau''_f}$$

$$\frac{dn_f}{dt} = -n_f\left(\frac{1}{\tau''_f} + \frac{1}{\tau'_x}\right) + \frac{n}{\tau'_f}$$

$$\frac{dn_s}{dt} = \frac{n_f}{\tau'_x}$$

At $t = 0$, $n = N$, $n_f = n_s = 0$

We assume further that

$$\tau'_f \ll \tau''_f, \tau'_x$$

let

$$x(t) = \begin{bmatrix} n \\ n_f \\ n_s \end{bmatrix}$$

Then the system of equations above becomes

$$x' = A\,x \quad , \quad x(0) = \begin{bmatrix} N \\ 0 \\ 0 \end{bmatrix}$$

where

$$A = \begin{bmatrix} -\frac{1}{\tau'_f} & \frac{1}{\tau''_f} & 0 \\ \frac{1}{\tau'_f} & -(\frac{1}{\tau''_f} + \frac{1}{\tau'_x}) & 0 \\ 0 & \frac{1}{\tau'_x} & 0 \end{bmatrix}$$

The solution for n(t) is

$$n(t) \simeq N\, e^{\lambda_1 t} + N \frac{\tau'_f}{\bar{\tau}}\, e^{\lambda_2 t}$$

with

$$\lambda_1 \simeq -\frac{1}{\tau'_f}$$

$$\lambda_2 \simeq -\frac{1}{\tau'_x}$$

$$\bar{\tau} = \frac{\tau''_f\ \tau'_x}{\tau''_f + \tau'_x}$$

Hence

$$J(t) \simeq J_{sc} e^{\lambda_1 t} + J_{sc} \frac{\tau'_f}{\bar{\tau}}\, e^{\lambda_2 t}$$

The ratio r of the initial amplitudes of the slow to the fast exponentials is

$$r \simeq \frac{\tau'_f}{\bar{\tau}} << 1$$

The detrapping process of model 1 which corresponds to the detrapping experiment performed at $77^{o}K$ is governed by the system

$$\frac{dn}{dt} = \frac{n_f}{\tau''_f}$$

$$\frac{dn_f}{dt} = -\frac{n_f}{\tau''_f} - \frac{n_f}{\tau'_x}$$

$$\frac{dn_s}{dt} = \frac{n_f}{\tau'_x}$$

At $t = 0$, $n_f = N$, $n_s = n = 0$

The solution is

$$n(t) = N \frac{\bar{\tau}}{\tau''_f} (1 - e^{-t/\bar{\tau}})$$

$$n_s(t) = N \frac{\bar{\tau}}{\tau'_x} (1 - e^{-t/\bar{\tau}})$$

where $$\bar{\tau} = \frac{\tau''_f \quad \tau'_x}{\tau''_f + \tau'_x}$$

The amount $\frac{\bar{\tau}}{\tau''_f} N$ is detrapped.

Consider the trapping process in model 2. The differential equations are

$$\frac{dn}{dt} = - n \left(\frac{1}{\tau'_f} + \frac{1}{\tau'_s}\right) + \frac{n_f}{\tau''_f}$$

$$\frac{dn_f}{dt} = \frac{n}{\tau'_f} - \frac{n_f}{\tau''_f}$$

$$\frac{dn_s}{dt} = \frac{n}{\tau'_s}$$

At $t = 0$, $n = N$, $n_f = n_s = 0$

We assume further that

$$\tau'_f << \tau''_f , \tau'_s$$

With

$$x(t) = \begin{bmatrix} n \\ n_f \\ n_s \end{bmatrix} , \quad x(0) = \begin{bmatrix} N \\ 0 \\ 0 \end{bmatrix}$$

we obtain

$$x' = Ax$$

where

$$A = \begin{bmatrix} -\left(\frac{1}{\tau'_f} + \frac{1}{\tau'_s}\right) & \frac{1}{\tau''_f} & 0 \\ \frac{1}{\tau'_f} & -\frac{1}{\tau''_f} & 0 \\ \frac{1}{\tau'_s} & 0 & 0 \end{bmatrix}$$

The solution for n(t) is

$$n(t) \simeq N e^{\lambda_1 t} + N \frac{\tau'_f}{\tau''_f} e^{\lambda_2 t}$$

where

$$\lambda_1 \simeq -\frac{1}{\tau'_f} \quad , \quad \lambda_2 \simeq -\frac{1}{\tau'_s}$$

Hence

$$J(t) \simeq J_{sc} e^{\lambda_1 t} + J_{sc} \frac{\tau'_f}{\tau''_f} e^{\lambda_2 t}$$

The ratio r of the initial amplitudes of the slow to the fast exponentials is

$$r \simeq \frac{\tau'_f}{\tau''_f} = \theta_f << 1$$

The corresponding detrapping process of model 2 involves only τ''_f, hence we expect all trapped charge to be detrapped.

The difference in the two models shows up in the results of the detrapping experiments: in model 1, only a fraction of the trapped injected charge escapes while in model 2, all of the trapped injected charge do. This feature is used to choose the correct model to be applied to our case.

In the calculations of the detrapping processes above, we have assumed that all carriers in the band are swept out before they could be retrapped again. This assumption is valid as long as the carrier transit time in the internal field generated by trapped charge is much smaller than the fastest trapping time. Just after the applied voltage pulse V_a is turned off (and the device is short-circuited), the average transit time t'_o is equal to $2t_o$ where $t_o = W^2/\mu V_a$ (W is the thickness of the device). As trapped charges are detrapped exponentially with time, the built-in field decreases, hence t'_o increases exponentially with time as well. The fastest trapping time encountered is

$$\tau'_f \simeq 3\mu s \quad .$$

A typical value for t_o is

$$t_o \simeq 1 \times 10^{-8} \text{ s.}$$

Hence

$$t_o' \simeq 2 \times 10^{-8} \exp (t/\tau')$$

where τ'' is the detrapping time constant. For $t_{short} \simeq 4\ \tau''$, t_o' will be around 3μs. Hence we expect the assumption that detrapped carriers are swept out before they could be retrapped again to be valid up to times $t_{short} \simeq 4\ \tau''$. Therefore our detrapping calculations are valid for a time period shorter than a few detrapping time constants.

In the detrapping experiment made in the temperature range $200^oK < T < 293^oK$, the only significant energy levels available to the carriers are the traps at 0.47 eV and the conduction band. The 0.14 eV level is too shallow at these temperatures to affect the detrapping process. At steady state, detailed balancing requires

$$n/\tau'_s = n_s/\tau''_s$$

or

$$\tau'_s/\tau''_s = n/n_s$$

Though for most of the temperature range considered, Boltzmann's statistics does not quite hold, we can still derive meaningful quantities by setting

$$\tau'_s/\tau''_s = (N_c/N_t)\exp(-E_t/kT) = \theta_s$$

Hence

$$1/\tau''_s = \frac{1}{\tau'_s}\ \frac{N_c}{N_t}\ \exp\ (-0.47/kT)$$

The average trapping time τ'_s can be measured experimentally, then τ''_s can be calculated. $\tau'_{s\ meas}$, $\tau''_{s\ meas}$ and $\tau''_{s\ calc}$ are tabulated in in table III in Section 3.3.4.

APPENDIX II

Ohmic and Transition Ranges of the Characteristics

Before Irradiation:

In section 2.1.3, it is observed from Hall effect measurements that, before irradiation, some portions of the silicon ingot used in this work show the presence of deep levels that reduce the free carrier concentration at $77^{o}K$ compared to that at room temperature. Such a distinction can also be observed among the n^{+} ν n^{+} devices.

Figs. 25 and 26 show typical DC and initial current J(V) characteristics in the Ohmic and transition ranges at room temperature and $77^{o}K$ for a device relatively free of deep levels. The free carrier concentration at room temperature as computed from the relation $R = W/(n_{o}q\mu A)$ is $n_{o} \simeq 7.7 \times 10^{11} cm^{-3}$ taking $\mu = 1500\ cm^{2}/Vs$, which is the value obtained from the square law asymptote. We note that, at room temperature, initial current densities (open symbols) are indistinguishable from current densities measured with DC (full symbols). This indicates that there is no trapping. At $77^{o}K$, the free carrier concentration in the dark, computed in the same way as at room temperature, is $n_{o} \simeq 2.7 \times 10^{11}\ cm^{-3}$ which is a factor of around 2 smaller than the value at room temperature. In these calculations of n_{o}, we have neglected the edge effects which could be significant since the Debye length at these concentrations is of the order of a few microns.

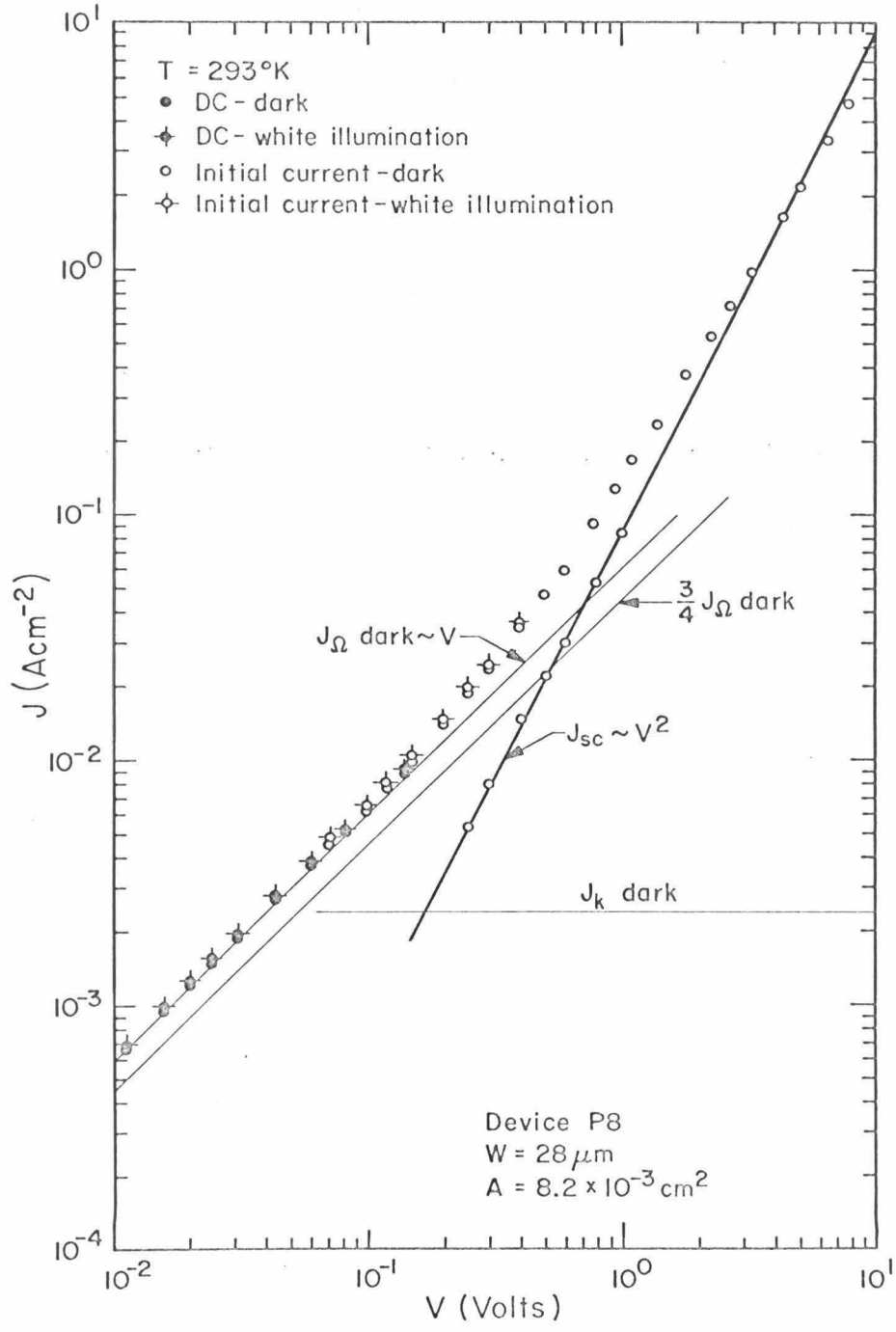

Figure 25 J(V) characteristics (initial current and DC) at low voltages of an unirradiated device at 293°K, made from the low resistivity portion of the original crystal, showing no trapping. The subtraction procedure is applied to the data obtained, yielding a well-defined square law asymptote.

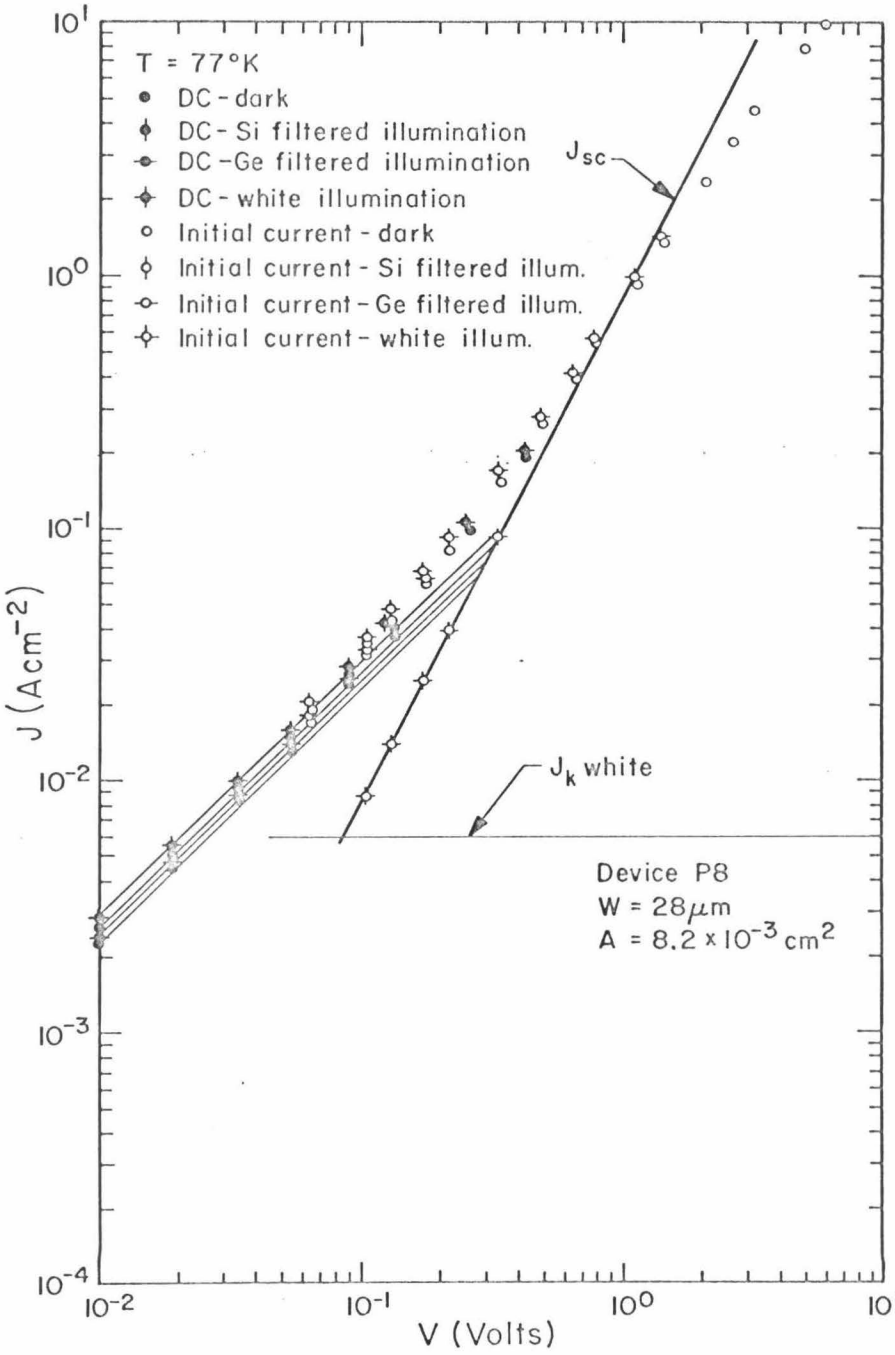

Figure 26 J(V) characteristics (initial current and DC) at low voltages of an unirradiated device at 77°K, made from the low resistivity portion of the original crystal, showing negligible trapping.

Trapping at $77^{o}K$ (observed as the difference between DC and initial current measurements in the transition and sclc ranges) is less than 5% and thus negligible.

Figs. 27 and 28 show the J(V) characteristics of a device with noticeable trapping ($\sim$17% at $293^{o}K$ and $\sim$50% at $77^{o}K$). For this device, the free carrier concentrations at thermal equilibrium differ by about a factor of 10 between $T = 293^{o}K$ and $T = 77^{o}K$. Hence we note the correlation between trapping in the transition and scl ranges and the strong decrease in the free carrier concentration at thermal equilibrium as the temperature is lowered. In all cases, trapping before irradiation reduces the current in the scl range from its (trap-free) initial current value by at most 50%. Compared to trapping after irradiation which is orders of magnitude greater, we feel justified in neglecting whatever traps existed in the crystal before irradiation.

After Irradiation:

After irradiation, the initial (trap-free) current vs voltage at low temperatures exhibit a "threshold voltage" (Fig. 12). To study this feature at $77^{o}K$, the following ambient conditions have been applied.

a) dark with $\Delta t \simeq 10$ min., where Δt is the time interval between the instant at which the white light is turned off (see Section 2.3) while the device remains short-circuited and the time at which the voltage pulse is applied.

b) dark with $\Delta t \simeq 1$ s

c) constant illumination with Ge light

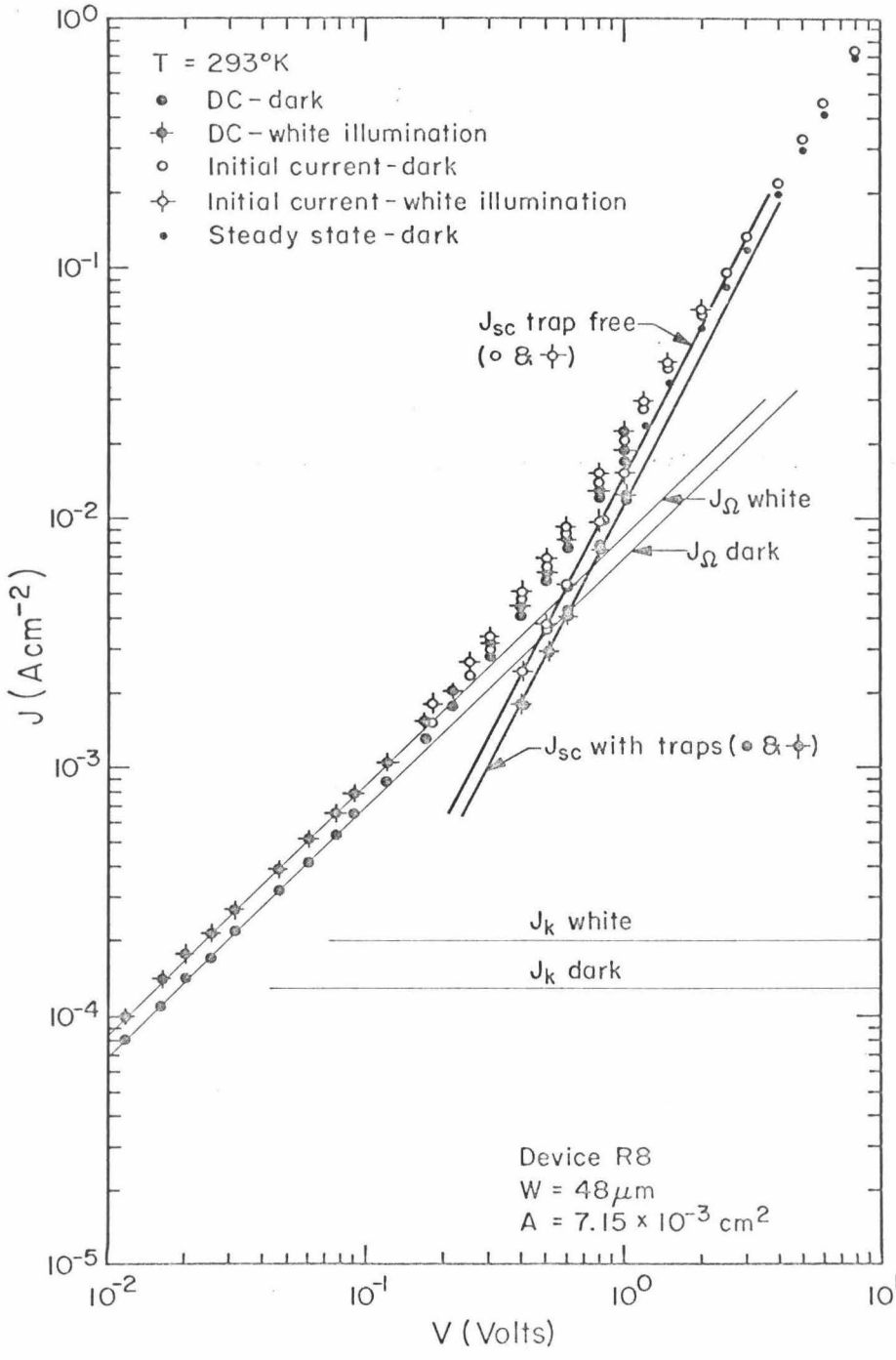

Figure 27 J(V) characteristics (initial current and DC) at low voltages of an unirradiated device at 293°K, made from the high resistivity portion of the original crystal, showing some trapping. The subtraction procedure is applied to the data obtained from DC and initial current measurements, yielding well-defined square law asymptotes.

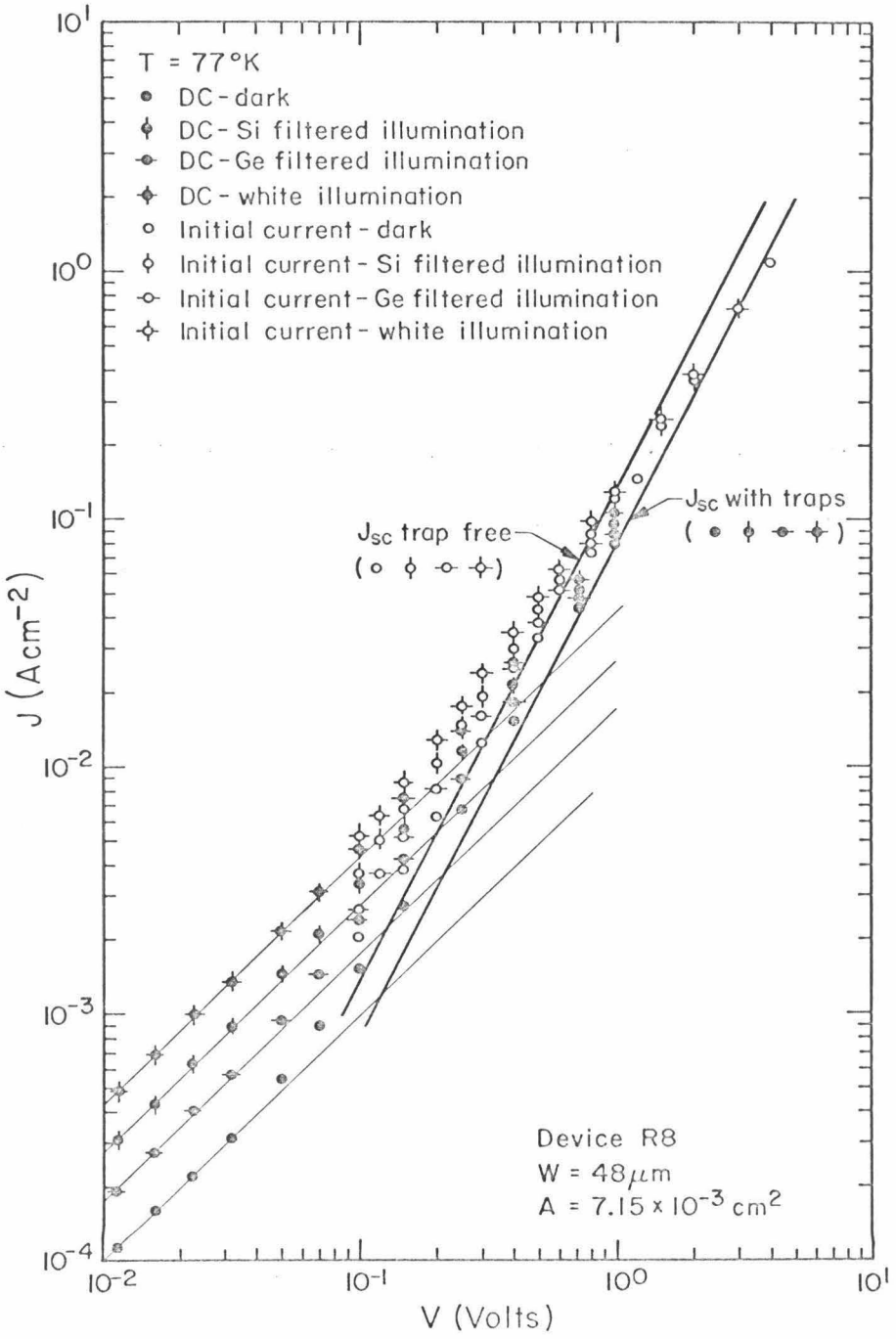

Figure 28 J(V) characteristics (initial current and DC) at low voltages of an unirradiated device at 77°K, made from the high resistivity portion of the original crystal, showing some trapping. Note the shift in the vertical axis compared to Figure 27.

d) constant illumination with Si light (see Fig. 21).

The results of these experiments indicate that the population at thermal equilibrium of free carriers in different levels is involved. The voltage at constant current density ($J = 10^{-3}$ A/cm^2) in this threshold range is plotted in function of device thickness in Fig. 29. A dependence very close to linear is observed. As noted in section 3.3.2, the situation encountered here is one in which the thermal equilibrium fermi level is one or two kT below the 0.47 eV level, and in which the free carrier concentration near the edges is determined by the contacts. A similar situation is discussed by Tredgold[12]. His computer calculations show that under such conditions, the current can increase faster with voltage than V^2 and that, in this range, the voltage at constant current is linear with thickness. As Tredgold expresses it, this situation involves a "current carried by injected space charge but in which the limiting process is confined to the contact regions." Such a behavior is believed to hold in $SrTiO_3$[12]. The similarity between Tredgold's results and ours leads us to believe that the same mechanism is involved. More work will be required on this subject to uphold or refute this tentative explanation.

At room temperature, the Ohmic current in several devices has been measured before and after irradiation. From such measurements, the thermal equilibrium concentration of free carriers can be obtained. The results are listed in table V.

The free carrier concentration is seen to decrease at the dose of

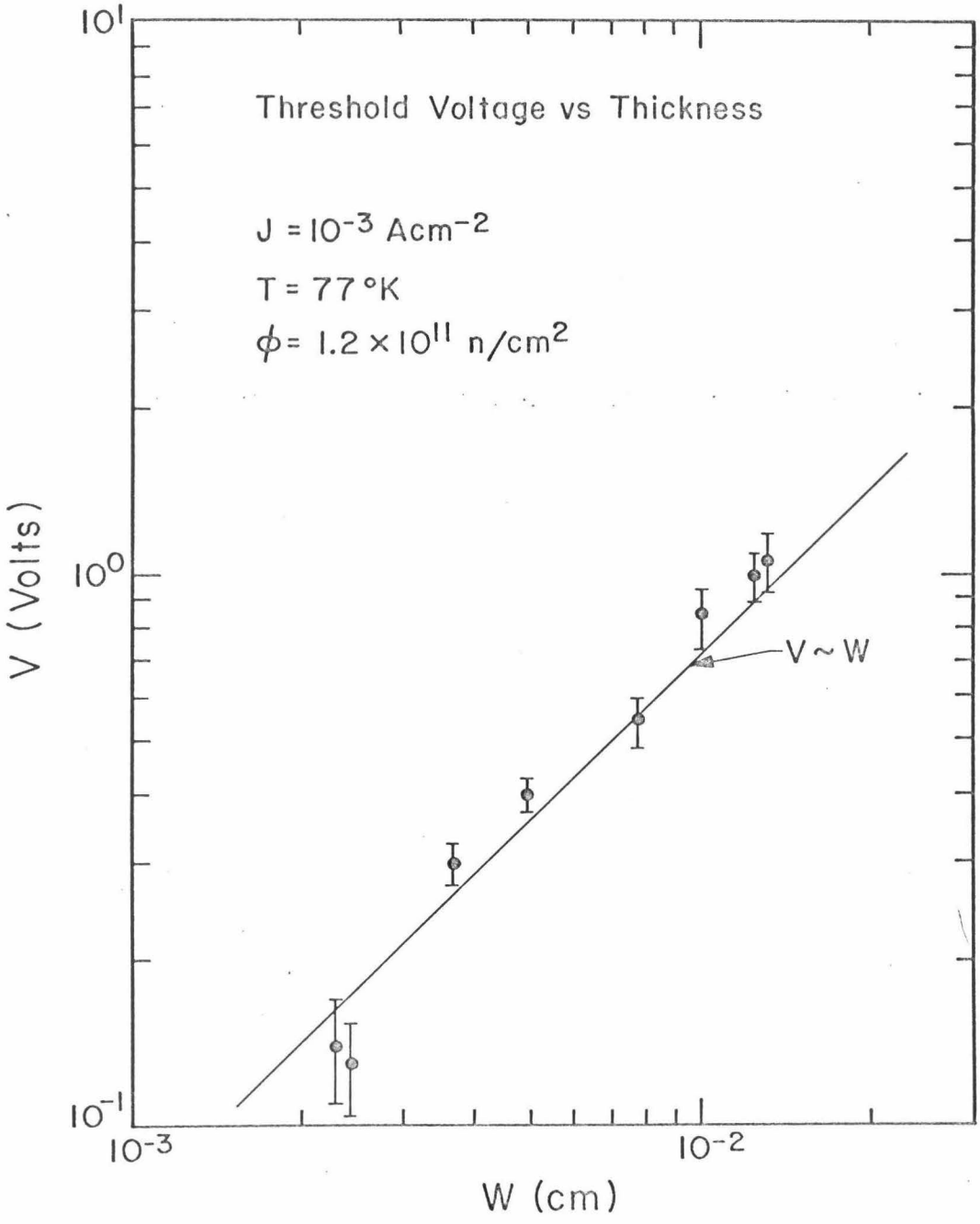

Figure 29 The dependence upon the thickness W of the voltage at a constant current density of J = 10^{-3}Acm^{-2} in the threshold voltage range of the initial current characteristics of devices at 77°K, in the dark and after irradiation at a dose of $\phi \approx 1.2 \times 10^{11}$n/cm^2.

TABLE V

Thermal Equilibrium Free Carrier Cencentration Before and After Irradiation as Measured From the Current in the Ohmic Range

Device	Thickness (μ)	Pre-irradiation concentration (cm^{-3})	Post-irradiation concentration (cm^{-3})
H2	130	7.8×10^{10}	3×10^{10}
L4	37	4.6×10^{11}	9×10^{10}
L6	24.5	7.1×10^{11}	3.6×10^{11}
I3	22.5	1.0×10^{12}	4×10^{11}

$\phi \simeq 1.2 \times 10^{11}$ n/cm^2. This decrease is due to a shift of the fermi level deeper into the band by the introduction of defect levels.

The Ohmic current after irradiation is plotted as a function of temperature in Fig. 30 for a thick (124μ) and a thin (24μ) device. After correcting for the temperature dependence of the mobility, assuming a one-carrier system (electron), we obtain the phenomenological relation

$$n_o \propto \exp(-0.2/kT)$$

independent of the device thickness. But such a temperature dependence at thermal equilibrium cannot be extracted from the model we have derived from the space-charge-limited range. It must be noted, however, that sclc is a situation very distinct from that of thermal equilibrium. In the space-charge-limited range, the electron concentration is many orders larger than that of thermal equilibrium, the hole concentration is therefore negligible and so are recombination-generation processes. At thermal equilibrium, however, these assumptions might not be valid. More work is needed to resolve this problem. Its solution would yield a direct way of relating thermal equilibrium data like Hall effect and resistivity measurements to our space-charge-limited current results.

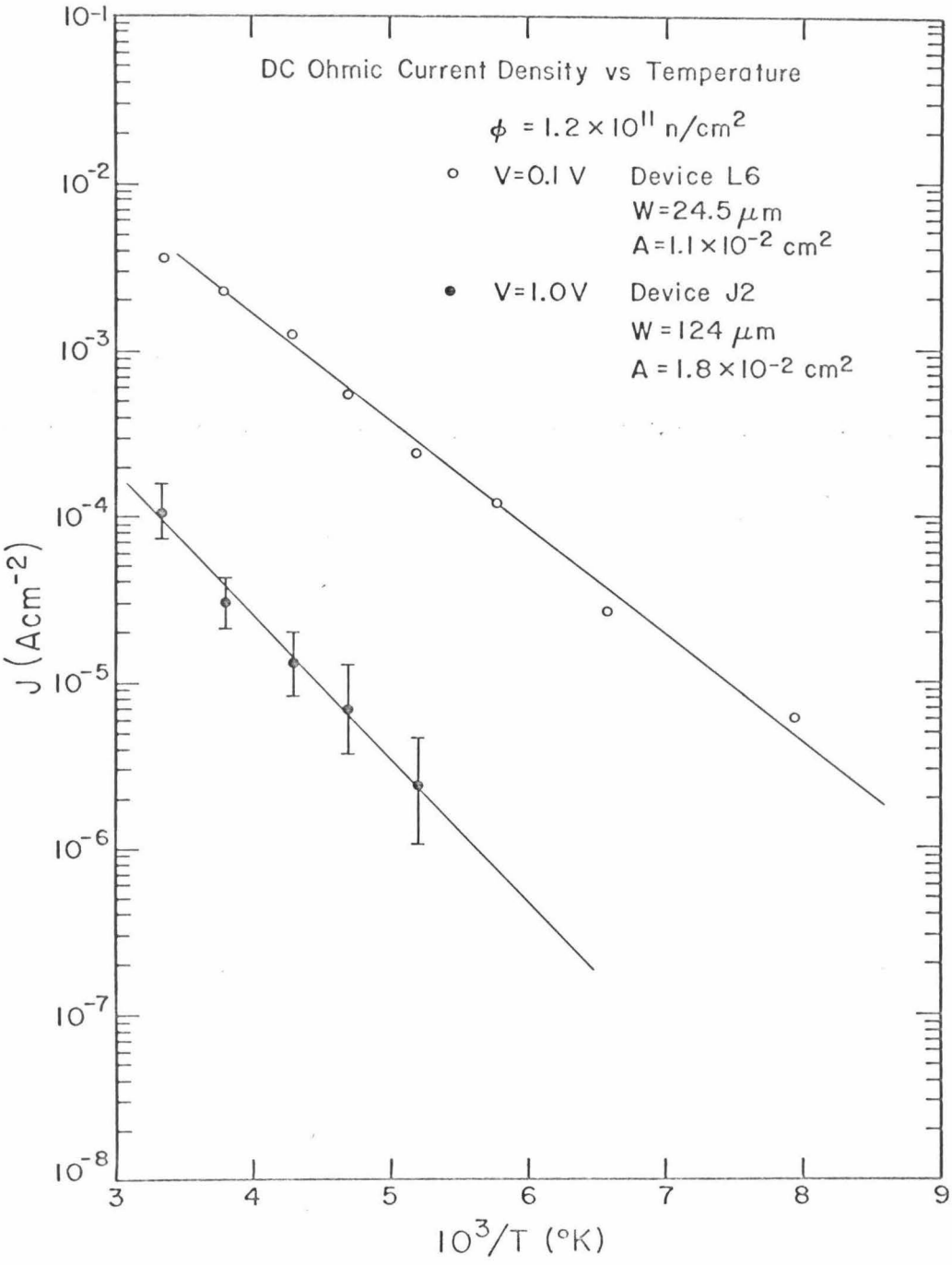

Figure 30 The dependence upon temperature of the DC current at a constant voltage in the Ohmic range for a thick and a thin device after irradiation at a dose of $\phi \approx 1.2 \times 10^{11}$ n/cm^2.

REFERENCES

1. M. A. Lampert et al., J. Phys. Chem. Solids 8, 464 (1959).
2. R. W. Smith and A. Rose, Phys. Rev. 97, 1531 (1955).
3. See for example S. Denda and M-A. Nicolet, J. Appl. Phys. 37, 2412 (1966).
4. A. Yamashita, Japan. J. Appl. Phys. 7, 1084 (1968).
5. M. A. Lampert, Phys. Rev. 103, 1648 (1956).
6. O. J. Marsh and C. R. Viswanathan, J. Appl. Phys. 38, 3135 (1967).
7. A. Rose, Phys. Rev. 97, 1538 (1955).
8. M. A. Lampert, Phys. Rev. 103, 1648 (1956).
9. A. Many and G. Rakavy, Phys. Rev. 126, 1980 (1962).
10. P. Mark and W. Helfrich, J. Appl. Phys. 33, 205 (1962).
11. B. L. Gregory and A. G. Jordan, Phys. Rev. 134, A1378 (1964).
12. R. H. Tredgold, Space Charge Conduction in Solids (Elsevier Publishing Company, Amsterdam, 1966) p.44.
13. H. R. Bilger and M-A. Nicolet, Rev. Sci. Inst. To be published.
14. V. Rodriguez and M-A. Nicolet, J. Appl. Phys. 40, 496 (1969).
15. J. F. Gibbons, IEEE Trans. on Electron Devices, ED-14, 37 (1967).
16. Private communication from R. D. Middlebrook.
17. B. L. Boichenko and V. M. Vasetskii, Fiz. Tverd. Tela 7, 2021 (1965) [English transl.: Soviet Phys. - Solid State 7, 1631 (1966)].
18. D. Long and J. Myers, Phys. Rev. 115, 1107 (1959).
19. C. Y. Duh and J. L. Moll, IEEE Trans. on Electron Dev. ED-14, 46 (1967).

20. B. R. Gossick, J. Appl. Phys. 30, 1214 (1959).

21. J. H. Crawford, Jr. and J. W. Cleland, J. Appl. Phys. 30, 1204 (1959).

22. G. T. Wright, Solid St. Electron. 2, 165 (1961).

23. A. Rose, Concepts in Photoconductivity and Allied Problems (Interscience Publishers, London, 1963) p. 123.

24. W. Ruppel and R. W. Smith, RCA Review 20, 702 (1959) -- W. Ruppel, Helvetica Physica Acta 31, 311 (1958).

25. B. L. Gregory, Appl. Phys. Lett. 16, 67 (1970).

26. V. S. Vavilov, A. F. Plotnikov, and V. D. Tkachev, Fiz. Tverd. Tela 4, 3446 (1963) [English transl.: Soviet Phys. - Solid State 4, 2522 (1963)].

27. H. J. Stein, Phys. Rev. 163, 801 (1967).

28. T. Tanaka and Y. Inuishi, J. Phys. Soc. Japan 19, 167 (1964).

29. R. F. Bass, Bull. Am. Phys. Soc. 11, 193 (1966).

30. O. L. Curtis, Jr., Bull. Am. Phys. Soc. 10, 739 (1965).

31. H. J. Stein, J. Appl. Phys. 37, 3382 (1966).